

The quark-meson coupling model for Λ , Σ and Ξ hypernuclei

K. Tsushima¹ ^{*}, K. Saito² [†], J. Haidenbauer³ [‡], and A. W. Thomas¹ [§]

¹Department of Physics and Mathematical Physics
and

Special Research Center for the Subatomic Structure of Matter,
University of Adelaide, SA 5005, Australia

²Physics Division, Tohoku College of Pharmacy, Sendai 981, Japan

³Forschungszentrum Jülich, IKP, D-52425 Jülich, Germany

December 2, 2024

Abstract

The quark-meson coupling (QMC) model, which has been successfully used to describe the properties of both infinite nuclear matter and finite nuclei, is applied to a systematic study of Λ , Σ and Ξ hypernuclei. Assumptions made in the present study are, (i) the (self-consistent) exchanged scalar, and vector, mesons couple only to the u and d quarks, and (ii) an SU(6) valence quark model for the bound nucleons and hyperon. The model automatically leads to a very weak spin-orbit interaction for the Λ in a hypernucleus. Effects of the Pauli blocking at the quark level, and the $\Sigma N - \Lambda N$ channel coupling (strong conversion), are also taken into account in a phenomenological way.

PACS: 12.39, 21.80, 24.10.J, 21.60.J, 71.25.J, 21.65

Keywords: The quark-meson coupling model, SU(6) quark model, Hypernuclei, Spin-orbit potential, Relativistic mean field, Effective mass

^{*}ktsushim@physics.adelaide.edu.au

[†]ksaito@nucl.phys.tohoku.ac.jp

[‡]j.haidenbauer@fz-juelich.de

[§]athomas@physics.adelaide.edu.au

1 Introduction

In earlier work [1, 2, 3] we addressed the question of whether quarks play an important role in finite nuclei. This involved quantitative investigations of the properties of closed-shell nuclei from ^{16}O to ^{208}Pb [1, 2], as well as the effective mass of the ρ meson formed in light nuclei [3]. These calculations were performed within the quark-meson coupling (QMC) model, originally suggested by Guichon [4], and with an extended version [3], which treats also the ω and ρ meson mass variations self-consistently in the medium.

In the QMC model, the interactions between hadrons are mediated by the exchange of scalar (σ) and vector (ω and ρ) mesons self-consistently coupled to the quarks within those hadrons. Within the model it has proven possible to successfully describe the properties of infinite nuclear matter [4, 5] and also finite nuclei [1, 2, 3]. Blunden and Miller [6], and Jin and Jennings [7] have made similar studies based on the QMC model, and some phenomenological extensions. One of the most attractive features of the QMC model is that it does not involve much in the way of additional complications to Quantum Hadrodynamics (QHD) [8]. Furthermore, it produces a reasonable value for the nuclear incompressibility [1]-[7].

Here we apply the QMC model [1, 2] to a systematic study of the properties of Λ , Σ and Ξ hypernuclei. Some of the initial results for Λ hypernuclei were reported already [9]. One of the purposes of the present article is to present the spin-orbit potentials for the hyperon calculated self-consistently with an explicit quark structure for the bound hyperon in the QMC model. These spin-orbit potentials generally contain anomalous contributions from the quarks due to the finite size of the hyperon.

Within the Born-Oppenheimer approximation, one can derive equations of motion for a hypernucleus in the QMC model [9] in the same way as has been done for normal nuclei [1, 2]. Such an approach may provide us with important information about the hyperon-nucleon interaction, the deep nuclear interior and a possible manifestation of the quark degrees of freedom via the Pauli principle at the quark level [10]-[65]. Below, we will briefly review the present situation regarding Λ hypernuclei first, because they have been well studied, both experimentally and theoretically.

As an example, the very weak spin-orbit interaction for Λ hypernuclei, which had been phenomenologically suggested by Bouyssy and Hüfner [10], was first explained by Brockman and Weise [11] in a relativistic Hartree model, and directly confirmed later by experiment [12]. However, a very strong SU(3) breaking effect was required to achieve this small spin-orbit force. An explanation in terms of quark and gluon dynamics was made by Pirner [13]. Alternatively, Noble [14] showed that this small spin-orbit force could be also realized without any large breaking of SU(3) symmetry, if an $\omega\Lambda\Lambda$ tensor coupling was introduced, analogous to the anomalous magnetic moment of the Λ . However, Dover and Gal [15] questioned whether the tensor coupling of the ω meson to the Λ could be related to the anomalous magnetic moment, because the spin of Λ is entirely carried by the s quark in a naive SU(6) valence quark model, and this s quark couples exclusively to the ϕ meson according to the OZI rule. Later, Jennings [16] pointed out that within Dirac phenomenology the tensor coupling of the ω meson to the Λ could be introduced in such a way as to guarantee that the direct ω coupling to the spin of the Λ was zero – as one would expect from a simple quark model. The resulting spin-orbit force agrees with the result obtained in the present model [9], on the basis of an explicit treatment of the quark structure of the Λ moving in vector and scalar fields that vary in space.

As a second example, it has also been discovered that there is an overbinding problem in the light Λ hypernuclei, and the existence of a repulsive core or the necessity of a repulsive three-body force have been suggested to overcome the problem [17]. The origin of this overbinding,

which could not be explained easily in terms of traditional nuclear physics, was ascribed to the Pauli principle at the quark level by Hungerford and Biedenharn [18]. Investigations of this repulsive core in the Λ -nucleus system have been made by Takeuchi and Shimizu, and others [19, 20], based on a nonrelativistic quark model.

In addition to the investigations of Λ hypernuclei, many studies of Σ and Ξ hypernuclei have been also made [15],[23]-[26],[40]-[65]. In particular, experiments on Σ hypernuclei performed at CERN [58], Brookhaven [59] and KEK [65], confirmed the existence of Σ hypernuclei. The former two experiments were done using K^- beams in so called “in-flight kinematics”, while the latter was done using stopped kaons. These experiments revealed an interesting feature of Σ hypernuclei, namely, the widths of the Σ in a hypernucleus seems to be narrower than the naive expectations due to the strong $\Sigma N - \Lambda N$ conversion (channel coupling). As for the Ξ hypernuclei, although not so many experiments on the double strangeness hypernuclei ($S = -2$) have been performed so far [60]-[63], there is a renewed interest in connection with the H dibaryon suggested by Jaffe [69], based on quark degrees of freedom – using the MIT bag model. Thus, we expect that more experiments on the Σ and Ξ hypernuclei, with higher statistics and precision, will be performed in the near future.

In the light of these investigations, it now seems appropriate to investigate the (heavier) hypernuclear systems, Λ , Σ and Ξ hypernuclei quantitatively, using a microscopic model based on quark degrees of freedom. For this purpose, the QMC model (which is built explicitly on quark degrees of freedom) seems ideally suited, because it has already been shown to describe the properties of finite nuclei quantitatively. The present investigation is one of the natural extensions of the study of quark degrees of freedom in finite nuclei.

The organization of the paper is as follows. In Section 2, the relativistic formulation of the hypernuclear system in QMC will be explained. A mean-field Lagrangian density and equations of motion will be derived in Section 2.1. Hyperons in infinite nuclear matter will be discussed in Section 2.2, while (finite) hypernuclei will be treated in Section 2.3. In Section 3, the spin-orbit potential for the hyperon in the QMC model will be discussed. Some results for hypernuclei in the QMC model alone will be given in Section 4. In Section 5, modifications necessary for a more realistic calculation in addition to the present version of the QMC model will be discussed. Effects of the Pauli blocking at the quark level, and the $\Lambda N - \Sigma N$ (and $\Xi N - \Lambda \Lambda$) channel coupling, will be considered in specific ways at the hadronic level in Sections 5.1, and 5.2, respectively. The results with including these effects discussed in Sections 5.1 and 5.2 will be given in Section 5.3. Finally, Section 6 will be devoted for summary and discussion.

2 Hypernuclei in the QMC model

In this Section, we will derive mean-field equations of motion for a hypernucleus, as well as consider a hyperon in nuclear matter.

2.1 Mean-field equations of motion

Using the Born-Oppenheimer approximation one can derive mean-field equations of motion for a hypernucleus in which the quasi-particles moving in single-particle orbits are three-quark clusters with the quantum numbers of a hyperon or a nucleon. One can then construct a relativistic Lagrangian density at the hadronic level [1, 2, 9], similar to that obtained in QHD [8], which produces the same equations of motion when expanded to the same order in velocity, v :

$$\mathcal{L}_{QMC}^{HY} = \mathcal{L}_{QMC} + \mathcal{L}_{QMC}^Y,$$

$$\begin{aligned}
\mathcal{L}_{QMC} &= \bar{\psi}_N(\vec{r}) \left[i\gamma \cdot \partial - M_N^*(\sigma) - (g_\omega \omega(\vec{r}) + g_\rho \frac{\tau_3^N}{2} b(\vec{r}) + \frac{e}{2}(1 + \tau_3^N) A(\vec{r})) \gamma_0 \right] \psi_N(\vec{r}) \\
&- \frac{1}{2}[(\nabla \sigma(\vec{r}))^2 + m_\sigma^2 \sigma(\vec{r})^2] + \frac{1}{2}[(\nabla \omega(\vec{r}))^2 + m_\omega^2 \omega(\vec{r})^2] \\
&+ \frac{1}{2}[(\nabla b(\vec{r}))^2 + m_\rho^2 b(\vec{r})^2] + \frac{1}{2}(\nabla A(\vec{r}))^2, \\
\mathcal{L}_{QMC}^Y &= \sum_{Y=\Lambda, \Sigma, \Xi} \bar{\psi}_Y(\vec{r}) \left[i\gamma \cdot \partial - M_Y^*(\sigma) - (g_\omega^Y \omega(\vec{r}) + g_\rho^Y I_3^Y b(\vec{r}) + e Q_Y A(\vec{r})) \gamma_0 \right] \psi_Y(\vec{r}),
\end{aligned} \quad (1)$$

where $\psi_N(\vec{r})$ ($\psi_Y(\vec{r})$) and $b(\vec{r})$ are respectively the nucleon (hyperon) and the ρ meson (the time component in the third direction of isospin) fields, while m_σ , m_ω and m_ρ are the masses of the σ , ω and ρ mesons. g_ω and g_ρ are the ω -N and ρ -N coupling constants which are related to the corresponding (u,d)-quark- ω , g_ω^q , and (u,d)-quark- ρ , g_ρ^q , coupling constants as $g_\omega = 3g_\omega^q$ and $g_\rho = g_\rho^q$ [1, 2].

In an approximation where the σ , ω and ρ mesons couple only to the u and d quarks (ideal mixing of the ω and ϕ mesons, and the OZI rule are assumed), the coupling constants in the hyperon sector are obtained as $g_\omega^Y = (n_0/3)g_\omega$, and $g_\rho^Y = g_\rho = g_\rho^q$, with n_0 being the total number of valence u and d quarks in the hyperon Y . I_3^Y and Q_Y are the third component of the hyperon isospin operator and its electric charge in units of the proton charge, e , respectively. The field dependent σ -N and σ -Y coupling strengths predicted by the QMC model, $g_\sigma(\sigma)$ and $g_\sigma^Y(\sigma)$, related to the Lagrangian density Eq. (1) at the hadronic level, are defined by:

$$M_N^*(\sigma) \equiv M_N - g_\sigma(\sigma) \sigma(\vec{r}), \quad (2)$$

$$M_Y^*(\sigma) \equiv M_Y - g_\sigma^Y(\sigma) \sigma(\vec{r}), \quad (3)$$

where M_N (M_Y) is the free nucleon (hyperon) mass. Note that the dependence of these coupling strengths on the applied scalar field must be calculated self-consistently within the quark model. Hence, unlike QHD, even though $g_\sigma^Y(\sigma)/g_\sigma(\sigma)$ may be 2/3 in free space ($\sigma = 0$)¹, this will not necessarily be the case in nuclear matter. More explicit expressions for $g_\sigma^Y(\sigma)$ and $g_\sigma(\sigma)$ will be given later. From the Lagrangian density Eq. (1), one gets a set of equations of motion for the hypernuclear system:

$$[i\gamma \cdot \partial - M_N^*(\sigma) - (g_\omega \omega(\vec{r}) + g_\rho \frac{\tau_3^N}{2} b(\vec{r}) + \frac{e}{2}(1 + \tau_3^N) A(\vec{r})) \gamma_0] \psi_N(\vec{r}) = 0, \quad (4)$$

$$[i\gamma \cdot \partial - M_Y^*(\sigma) - (g_\omega^Y \omega(\vec{r}) + g_\rho^Y I_3^Y b(\vec{r}) + e Q_Y A(\vec{r})) \gamma_0] \psi_Y(\vec{r}) = 0, \quad (5)$$

$$\begin{aligned}
(-\nabla_r^2 + m_\sigma^2) \sigma(\vec{r}) &= -[\frac{\partial M_N^*(\sigma)}{\partial \sigma}] \rho_s(\vec{r}) - [\frac{\partial M_Y^*(\sigma)}{\partial \sigma}] \rho_s^Y(\vec{r}), \\
&\equiv g_\sigma C_N(\sigma) \rho_s(\vec{r}) + g_\sigma^Y C_Y(\sigma) \rho_s^Y(\vec{r}),
\end{aligned} \quad (6)$$

$$(-\nabla_r^2 + m_\omega^2) \omega(\vec{r}) = g_\omega \rho_B(\vec{r}) + g_\omega^Y \rho_B^Y(\vec{r}), \quad (7)$$

$$(-\nabla_r^2 + m_\rho^2) b(\vec{r}) = \frac{g_\rho}{2} \rho_3(\vec{r}) + g_\rho^Y I_3^Y \rho_B^Y(\vec{r}), \quad (8)$$

$$(-\nabla_r^2) A(\vec{r}) = e \rho_p(\vec{r}) + e Q_Y \rho_B^Y(\vec{r}), \quad (9)$$

where, $\rho_s(\vec{r})$ ($\rho_s^Y(\vec{r})$), $\rho_B(\vec{r})$ ($\rho_B^Y(\vec{r})$), $\rho_3(\vec{r})$ and $\rho_p(\vec{r})$ are the scalar, baryon, third component of isovector, and proton densities at the position \vec{r} in the hypernucleus [2, 3]. On the right hand side of Eq. (6), a new, and characteristic feature of QMC beyond QHD [8, 39, 42] appears,

¹Strictly, this is true only when the bag radii of nucleon and hyperon are exactly the same in the present model. See Eq. (13), below.

namely, $-\frac{\partial M_N^*(\sigma)}{\partial \sigma} = g_\sigma C_N(\sigma)$ and $-\frac{\partial M_Y^*(\sigma)}{\partial \sigma} = g_\sigma^Y C_Y(\sigma)$, where $g_\sigma \equiv g_\sigma(\sigma = 0)$ and $g_\sigma^Y \equiv g_\sigma^Y(\sigma = 0)$. The effective mass for the hyperon Y is defined by

$$M_Y^*(\sigma) = \frac{n_0 \Omega^*(\sigma) + (3 - n_0) \Omega_s^* - z_Y}{R_Y} + \frac{4}{3} \pi (R_Y)^3 B, \quad (10)$$

with the MIT bag model quantities [1, 2]

$$S_Y(\sigma) = \frac{\Omega^*(\sigma)/2 + m_{u,d}^*(\sigma) R_Y (\Omega^*(\sigma) - 1)}{\Omega^*(\sigma)(\Omega^*(\sigma) - 1) + m_{u,d}^*(\sigma) R_Y/2}, \quad (11)$$

$$C_Y(\sigma) = S_Y(\sigma)/S_Y(0), \quad (12)$$

$$g_\sigma^Y \equiv n_0 g_\sigma^q S_Y(0) = \frac{n_0}{3} g_\sigma S_Y(0)/S_N(0) \equiv \frac{n_0}{3} g_\sigma \Gamma_{Y/N}, \quad (13)$$

$$\Omega^*(\sigma) = \sqrt{x^2 + (R_Y m_{u,d}^*(\sigma))^2}, \quad \Omega_s^* = \sqrt{x_s^2 + (R_Y m_s)^2}, \quad (14)$$

$$m_{u,d}^*(\sigma) = m_{u,d} - g_\sigma^q \sigma(\vec{r}), \quad (15)$$

such R_Y that satisfies

$$\left. \frac{dM_Y^*(\sigma)}{dR_Y} \right|_{R_Y=R_Y^*} = 0. \quad (16)$$

The density dependent σ -Y coupling constant is defined by

$$\frac{\partial M_Y^*(\sigma)}{\partial \sigma} = -n_0 g_\sigma^q \int_{\text{bag}} d\vec{y} \bar{\psi}_{u,d}(\vec{y}) \psi_{u,d}(\vec{y}) \equiv -n_0 g_\sigma^q S_Y(\sigma) = -\frac{\partial}{\partial \sigma} [g_\sigma^Y(\sigma) \sigma]. \quad (17)$$

For the nucleon, replace the suffix Y by N in Eqs. (10) - (17) and set $n_0 = 3$. Here, z_Y , B , x , x_s and $m_{u,d,s}$ are the parameters for the sum of the c.m. and gluon fluctuation effects, bag pressure, lowest eigenvalues for the (u, d) and s quarks, respectively, and the corresponding current quark masses with $m_u = m_d$. z_N and B (z_Y) are fixed by fitting the nucleon (hyperon) mass in free space. The bag parameters calculated and chosen for the present study are, $R_N = 0.8$ fm (in free space), $B = (170 \text{ MeV})^4$, $m_u = m_d = 5$ MeV and $m_s = 250$ MeV. Note that due to the equilibrium condition Eq. (16), which is applied also to the free nucleonic vacuum, the bag radius for each hyperon in free space is slightly different. The parameters $z_{N,Y}$ and the bag radii, $R_{N,Y}$, obtained by fitting to their physical masses in free space are listed in Table 1.

Table 1: The bag parameters, $z_{N,Y}$, the bag radii in free space, $R_{N,Y}$ and the physical baryon masses fitted in free space. They are obtained with the bag pressure, $B = (170 \text{ MeV})^4$, current quark masses, $m_u = m_d = 5$ MeV and $m_s = 250$ MeV.

	mass (MeV)	$z_{N,Y}$	$R_{N,Y}$ (fm)
N	939.0	3.295	0.800
Λ	1115.7	3.131	0.806
Σ	1193.1	2.810	0.827
Ξ	1318.1	2.860	0.820

The parameters associated with the u and d quarks are those found in our previous investigations [2]. The value for the mass of the s quark was chosen to be 250 MeV. We note that the final results are insensitive to this parameter. The value for $\Gamma_{Y/N}$ in Eq. (13) turned

out to be almost unity for all hyperons even though $R_N \neq R_Y$ (see also Eqs. (11)), so we can use $\Gamma_{Y/N} = 1$ in practice [3]. Although the bag radii in free space for the nucleon and hyperons are slightly different ($R_N \neq R_Y$), they will be generically denoted by $R_B = 0.8$ fm in Figs. 1 and 2.

At the hadronic level, the entire information on the quark dynamics is condensed into the effective coupling $C_{N,Y}(\sigma)$ of Eq. (6), or Eq. (12). Furthermore, when $C_{N,Y}(\sigma) = 1$, which corresponds to a structureless nucleon or hyperon, the equations of motion given by Eqs. (4)-(9) can be identified with those derived from QHD [28, 39, 42], except for the terms arising from the tensor coupling and the non-linear scalar field interaction introduced beyond naive QHD.

2.2 Nuclear matter limit

Here, we consider a hyperon in nuclear matter. In this limit the meson fields become constants, and we denote the mean-value of the σ field as $\bar{\sigma}$. The self-consistency condition for the σ field, $\bar{\sigma}$, and effective nucleon mass, $M_N^*(\bar{\sigma})$, is given by [1, 2, 5]

$$\bar{\sigma} = \frac{g_\sigma}{m_\sigma^2} C_N(\bar{\sigma}) \frac{4}{(2\pi)^3} \int d\vec{k} \theta(k_F - k) \frac{M_N^*(\bar{\sigma})}{\sqrt{M_N^*(\bar{\sigma}) + \vec{k}^2}}, \quad (18)$$

where $g_\sigma = (3g_\sigma^q S_N(0))$, k_F is the Fermi momentum, and $C_N(\bar{\sigma})$ is now the constant value of C_N in the scalar field. Note that $M_N^*(\bar{\sigma})$, in Eq. (18), must be calculated self-consistently by the MIT bag model, through Eqs. (10) - (17). This self-consistency equation for $\bar{\sigma}$ is the same as that in QHD, except that in the latter model one has $C_N(\bar{\sigma}) = 1$ [8]. By using the obtained mean field value, $\bar{\sigma}$, the corresponding quantity for the hyperon Y , $C_Y(\bar{\sigma})$, can be also calculated using Eqs. (11) and (12), where the effect of a single hyperon on the mean field value, $\bar{\sigma}$, in infinite nuclear matter can be neglected. The calculated values of $C_{N,Y}(\bar{\sigma})$ for the nucleon and hyperons are displayed in Fig. 1. It has been found that the function $C_{N,Y}(\bar{\sigma})$ can

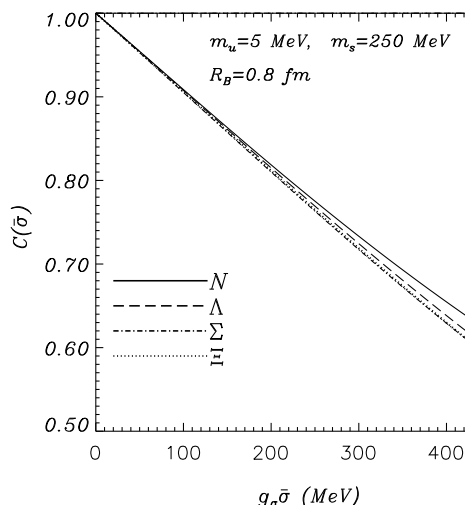


Figure 1: $C(\bar{\sigma})$ for nucleon and hyperons in nuclear matter.

be parametrized as a linear form in the σ field, $g_\sigma \bar{\sigma}$, for practical calculations [1, 2, 3] by

$$C_{N,Y}(\bar{\sigma}) = 1 - a_{N,Y} \times (g_\sigma \bar{\sigma}), \quad (19)$$

which can be also seen from Fig. 1, where $g_\sigma \bar{\sigma} = (3g_\sigma^q S_N(0)) \bar{\sigma}$ in MeV. The values of $a_{N,Y}$ for nucleon and hyperons are given in Table 2. This parametrization works very well up to about

Table 2: The slope parameters, a_N and a_Y .

	$\times 10^{-4} \text{ MeV}^{-1}$
a_N	8.8
a_Λ	9.3
a_Σ	9.5
a_Ξ	9.4

three times normal nuclear density, $\rho_B \simeq 3\rho_0$, with $\rho_0 \simeq 0.15 \text{ fm}^{-3}$. For the field strength, $g_\sigma \bar{\sigma}$, versus baryon density, see Ref. [1].

Next, we define the variations of effective masses for the baryon j ($j = N, \Lambda, \Sigma, \Xi$):

$$\delta M_j^* \equiv M_j - M_j^*, \quad (20)$$

which should be calculated self-consistently through the corresponding Eqs. (10)-(18). Calculated values for the variation of effective masses against baryon density are shown in Fig. 2. For the effective mass, M_j^* , one can write down explicit expressions using the parametrization

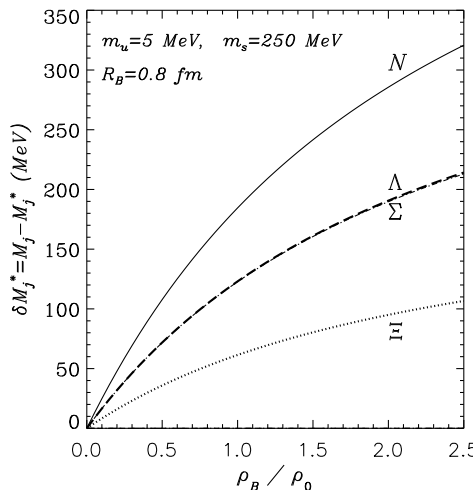


Figure 2: Variation of the effective masses for nucleon and hyperons in nuclear matter, where normal nuclear matter density, ρ_0 , is 0.15 fm^{-3} .

for $C_{N,Y}(\bar{\sigma})$ of Eq. (19):

$$\begin{aligned} M_N^* &\equiv M_N - g_\sigma(\bar{\sigma})\bar{\sigma} \simeq M_N - g_\sigma \left[1 - \frac{a_N}{2}(g_\sigma \bar{\sigma}) \right] \bar{\sigma}, \\ M_Y^* &\equiv M_Y - g_\sigma^Y(\bar{\sigma})\bar{\sigma} \simeq M_Y - \frac{n_0}{3}g_\sigma \left[1 - \frac{a_Y}{2}(g_\sigma \bar{\sigma}) \right] \bar{\sigma}. \end{aligned} \quad (21)$$

Because the parameters $a_{N,Y}$ are almost the same in magnitudes (See Table 2), we find a simple scaling relation for the variation of effective masses [3]:

$$\frac{\delta M_\Lambda^*}{\delta M_N^*} \simeq \frac{\delta M_\Sigma^*}{\delta M_N^*} \simeq \frac{2}{3}, \quad \frac{\delta M_{\Xi}^*}{\delta M_N^*} \simeq \frac{1}{3}. \quad (22)$$

This scaling relation is well demonstrated in Fig. 2. It is worth noting that the ratio of the effective mass to the bare mass, M_j^*/M_j , does not decrease linearly as the baryon density increases in the QMC model, which is different from the relation adopted by Kuwabara and Hatsuda [70], based on a model of the QHD type.

2.3 Hypernuclei

The variation of the Lagrangian density Eq. (1) results in the following equations for static, spherically symmetric nuclei plus one hyperon configuration (Hereafter, we will call this configuration simply a hypernucleus):

$$\frac{d^2}{dr^2}\sigma(r) + \frac{2}{r}\frac{d}{dr}\sigma(r) - m_\sigma^2\sigma(r) = -g_\sigma C_N(\sigma(r))\rho_s(r) - g_\sigma^Y C_Y(\sigma(r))\rho_s^Y(r), \quad (23)$$

$$\frac{d^2}{dr^2}\omega(r) + \frac{2}{r}\frac{d}{dr}\omega(r) - m_\omega^2\omega(r) = -g_\omega\rho_B(r) - g_\omega^Y\rho_B^Y(r), \quad (24)$$

$$\frac{d^2}{dr^2}b(r) + \frac{2}{r}\frac{d}{dr}b(r) - m_\rho^2b(r) = -\frac{g_\rho}{2}\rho_3(r) - g_\rho^Y t_\beta\rho_B^Y(r), \quad (25)$$

$$\frac{d^2}{dr^2}A(r) + \frac{2}{r}\frac{d}{dr}A(r) = -e\rho_p(r) - eQ_Y\rho_B^Y(r), \quad (26)$$

(27)

where

$$\rho_s(r) = \sum_{\alpha}^{occ} d_{\alpha}(r)(|G_{\alpha}(r)|^2 - |F_{\alpha}(r)|^2), \quad (28)$$

$$\rho_s^Y(r) = d_{\beta}(r)(|G_{\beta}(r)|^2 - |F_{\beta}(r)|^2), \quad (29)$$

$$\rho_B(r) = \sum_{\alpha}^{occ} d_{\alpha}(r)(|G_{\alpha}(r)|^2 + |F_{\alpha}(r)|^2), \quad (30)$$

$$\rho_B^Y(r) = d_{\beta}(r)(|G_{\beta}(r)|^2 + |F_{\beta}(r)|^2), \quad (31)$$

$$\rho_3(r) = \sum_{\alpha}^{occ} d_{\alpha}(r)(-)^{t_{\alpha}-1/2}(|G_{\alpha}(r)|^2 + |F_{\alpha}(r)|^2), \quad (32)$$

$$\rho_p(r) = \sum_{\alpha}^{occ} d_{\alpha}(r)(t_{\alpha} + \frac{1}{2})(|G_{\alpha}(r)|^2 + |F_{\alpha}(r)|^2), \quad (33)$$

with $d_{\alpha}(r) = (2j_{\alpha} + 1)/4\pi r^2$, $d_{\beta}(r) = 1/4\pi r^2$ and

$$\begin{aligned} \frac{d}{dr}G_{\alpha}(r) + \frac{\kappa}{r}G_{\alpha}(r) - [\epsilon_{\alpha} - g_{\omega}\omega(r) - t_{\alpha}g_{\rho}b(r) &- (t_{\alpha} + \frac{1}{2})eA(r) + M_N \\ &- g_{\sigma}(\sigma(r))\sigma(r)]F_{\alpha}(r) = 0, \end{aligned} \quad (34)$$

$$\begin{aligned} \frac{d}{dr}F_{\alpha}(r) - \frac{\kappa}{r}F_{\alpha}(r) + [\epsilon_{\alpha} - g_{\omega}\omega(r) - t_{\alpha}g_{\rho}b(r) &- (t_{\alpha} + \frac{1}{2})eA(r) - M_N \\ &+ g_{\sigma}(\sigma(r))\sigma(r)]G_{\alpha}(r) = 0, \end{aligned} \quad (35)$$

$$\begin{aligned} \frac{d}{dr}G_\beta(r) + \frac{\kappa}{r}G_\beta(r) - [\epsilon_\beta - g_\omega^Y \omega(r) - t_\beta g_\rho^Y b(r) &- eQ_Y A(r) + M_Y \\ &- g_\sigma^Y(\sigma(r))\sigma(r)] F_\beta(r) = 0, \end{aligned} \quad (36)$$

$$\begin{aligned} \frac{d}{dr}F_\beta(r) - \frac{\kappa}{r}F_\beta(r) + [\epsilon_\beta - g_\omega^Y \omega(r) - t_\beta g_\rho^Y b(r) &- eQ_Y A(r) - M_Y \\ &+ g_\sigma^Y(\sigma(r))\sigma(r)] G_\beta(r) = 0. \end{aligned} \quad (37)$$

Here $G_{\alpha,\beta}(r)/r$ and $F_{\alpha,\beta}(r)/r$ are respectively the radial part of the upper and lower components of the solution to the Dirac equation for the nucleon (hyperon) [8]:

$$\psi_{N,Y}(\vec{r}) = \begin{pmatrix} i[G_{\alpha,\beta}(r)/r]\Phi_{\kappa m} \\ -[F_{\alpha,\beta}(r)/r]\Phi_{-\kappa m} \end{pmatrix} \xi_{t_{\alpha,\beta}}, \quad (38)$$

where $\xi_{t_{\alpha,\beta}}$ is a two-component isospinor and $\Phi_{\kappa m}$ is a spin spherical harmonic for the nucleon (hyperon) [3] (α (β) labelling the quantum numbers of nucleon (hyperon) and $\epsilon_{\alpha,\beta}$ being the energies). Then, the normalization condition is,

$$\int dr(|G_{\alpha,\beta}(r)|^2 + |F_{\alpha,\beta}(r)|^2) = 1. \quad (39)$$

As usual, κ specifies the angular quantum numbers and t_α (t_β) the eigenvalue of the isospin operator $\tau_3^N/2$ (I_3^Y). The total energy of the hypernuclear system is then given by

$$\begin{aligned} E_{tot} = & \sum_{\alpha}^{occ} (2j_\alpha + 1)\epsilon_\alpha + \epsilon_\beta - \frac{1}{2} \int d\vec{r} [-g_\sigma C_N(\sigma(r))\sigma(r)\rho_s(r) \\ & + g_\omega \omega(r)\rho_B(r) + \frac{1}{2}g_\rho b(r)\rho_3(r) + eA(r)\rho_p(r)] \\ & - \frac{1}{2} \int d\vec{r} [-g_\sigma^Y C_Y(\sigma(r))\sigma(r)\rho_s^Y(r) \\ & + g_\omega^Y \omega(r)\rho_B^Y(r) + g_\rho^Y b(r)t_\beta \rho_B^Y(r) + eQ_Y A(r)\rho_B^Y(r)]. \end{aligned} \quad (40)$$

3 Spin-orbit potential in the QMC model

In this section, we will focus on the spin-orbit potential of a hyperon in a hypernucleus. In order to see the differences between the QMC model and the QHD type models, we first discuss the spin-orbit potential of the Λ .

The origin of the spin orbit force for a composite nucleon moving through scalar and vector fields which vary with position was explained in detail in Ref. [1] a) – cf. Section 3.2. The situation for the Λ is different in that, in an SU(6) quark model, the u and d quarks are coupled to spin zero, so that the spin of the Λ is carried by the s quark. As the σ -meson is viewed here as a convenient parametrization of two-pion-exchange and the ω and ρ are non-strange, it seems reasonable to assume that the σ , ω and ρ mesons couple only to the u and d quarks. The direct contributions to the spin-orbit interaction from these mesons (derived in Section 3 of Ref. [1] a)) then vanish due to the flavor-spin structure. Thus, the spin-orbit interaction, $V_{S.O.}^\Lambda(r)\vec{l}\cdot\vec{s}$, at the position \vec{r} of the Λ in a hypernucleus arises entirely from Thomas precession:

$$V_{S.O.}^\Lambda(r)\vec{l}\cdot\vec{s} = -\frac{1}{2}\vec{v}_\Lambda \times \frac{d\vec{v}_\Lambda}{dt} \cdot \vec{s} = -\frac{1}{2M_\Lambda^{*2}(r)r} \left(\frac{d}{dr}[M_\Lambda^*(r) + g_\omega^\Lambda \omega(r)] \right) \vec{l}\cdot\vec{s}, \quad (41)$$

where, $\vec{v}_\Lambda = \vec{p}_\Lambda/M_\Lambda^*$, is the velocity of the Λ in the rest frame of the Λ hypernucleus, and the acceleration, $d\vec{v}_\Lambda/dt$, is obtained from the Hamilton equations of motion applied to the leading order Hamiltonian of the QMC model [1]. Because the contributions from the effective mass of the Λ , $M_\Lambda^*(r)$, and the vector potential, $g_\omega^\Lambda \omega(r)$, are approximately equal and opposite in sign, we quite naturally expect a very small spin-orbit interaction for the Λ in the hypernucleus. Although the spin-orbit splittings for the nucleon calculated in QMC are already somewhat smaller [1, 2] than those calculated in QHD [8], we can expect much smaller spin-orbit splittings for the Λ in QMC, which will be confirmed numerically later. In order to include the spin-orbit potential of Eq. (41) correctly, we added perturbatively the correction due to the vector potential, $-\frac{2}{2M_\Lambda^{*2}(r)r} \left(\frac{d}{dr} g_\omega^\Lambda \omega(r) \right) \vec{l} \cdot \vec{s}$, to the single-particle energies obtained with the Dirac equation Eq. (5), by evaluating it with the obtained wave function for the Λ . This is necessary because the Dirac equation corresponding to Eq. (5) leads to a spin-orbit force which does not correspond to the underlying quark model, namely:

$$V_{S.O.}^\Lambda(r) \vec{l} \cdot \vec{s} = -\frac{1}{2M_\Lambda^{*2}(r)r} \left(\frac{d}{dr} [M_\Lambda^*(r) - g_\omega^\Lambda \omega(r)] \right) \vec{l} \cdot \vec{s}. \quad (42)$$

This correction to the spin-orbit force, which appears naturally in the QMC model, may also be modelled at the hadronic level of the Dirac equation by adding a tensor interaction.

In the QMC model, the general expression for the spin-orbit potential felt by the nucleon or hyperon, j ($j = N, \Lambda, \Sigma, \Xi$), may be expressed as

$$V_{S.O.}^j(r) \vec{l} \cdot \vec{s} = \frac{-1}{2M_j^{*2}(r)r} \left[\Delta_\sigma^j + (G_j^s - 6F_j^s \mu_s \eta_j(r)) \Delta_\omega^j + (G_j^v - \frac{6}{5}F_j^v \mu_v \eta_j(r)) \Delta_\rho^j \right] \vec{l} \cdot \vec{s}, \quad (43)$$

with

$$\Delta_\sigma^j = \frac{d}{dr} M_j^*(r), \quad \Delta_\omega^j = \frac{d}{dr} \left(\frac{n_0}{3} \right) g_\omega \omega(r), \quad \Delta_\rho^j = \frac{d}{dr} g_\rho b(r), \quad (44)$$

$$G_j^s = \langle j | \sum_{i=u,d} 1(i) | j \rangle, \quad G_j^v = \langle j | \sum_{i=u,d} \frac{1}{2} \tau_3(i) | j \rangle, \quad (45)$$

$$F_j^s = \frac{\langle j | \sum_{i=u,d} \frac{1}{2} \vec{\sigma}(i) | j \rangle}{\langle j | \frac{1}{2} \vec{\sigma}^j | j \rangle}, \quad F_j^v = \frac{\langle j | \sum_{i=u,d} \frac{1}{2} \vec{\sigma}(i) \frac{1}{2} \tau_3(i) | j \rangle}{\langle j | \frac{1}{2} \vec{\sigma}^j | j \rangle}, \quad (46)$$

$$\mu_s = \frac{1}{3} M_N I_0 = \frac{5}{3} \mu_v, \quad \eta_j(r) = \frac{I_j^* M_j^*(r)}{I_0 M_N}, \quad (47)$$

$$I_0 = \frac{R_N}{3} \frac{4\Omega_N + 2m_{u,d}R_N - 3}{2\Omega_N(\Omega_N - 1) + m_{u,d}R_N}, \quad (48)$$

$$I_j^* = \frac{R_j^*}{3} \frac{4\Omega_j^*(\sigma) + 2m_{u,d}^*(\sigma)R_j^* - 3}{2\Omega_j^*(\sigma)(\Omega_j^*(\sigma) - 1) + m_{u,d}^*(\sigma)R_j^*}. \quad (49)$$

Here \vec{r} is the position of the baryon j in the hypernucleus (nucleus), and the terms proportional to μ_s and μ_v are the anomalous contributions from the u and/or d quarks due to the finite size of the hyperon (nucleon). They are related to the magnetic moments of the proton, μ_p , and the neutron, μ_n , as $\mu_s = \mu_p + \mu_n$ and $\mu_v = \mu_p - \mu_n$, with the experimental values, $\mu_p = 2.79$ and $\mu_n = -1.91$ (in nuclear magnetons). However, these μ_s and μ_v , together with the quantities I_0 and I_j^* of Eqs. (48) and (49), must be, and will be calculated self-consistently in the model. Note that the in-medium bag radius, R_j^* , and the lowest bag eigenenergy for the u (d) quark,

Ω_j^* in units of $1/R_j^*$, depend on j ($j = N, \Lambda, \Sigma, \Xi$), because the bag radius is generally different for each iso-multiplet of the octet baryons in the medium. The explicit expressions for the spin-orbit potentials for the octet baryons in the QMC model are given by:

$$V_{S.O.}^p(r) = \frac{-1}{2M_N^{*2}(r)r} \left[\Delta_\sigma^N + (1 - 2\mu_s \eta_N(r)) \Delta_\omega^N + \frac{1}{2} (1 - 2\mu_v \eta_N(r)) \Delta_\rho \right], \quad (50)$$

$$V_{S.O.}^n(r) = \frac{-1}{2M_N^{*2}(r)r} \left[\Delta_\sigma^N + (1 - 2\mu_s \eta_N(r)) \Delta_\omega^N - \frac{1}{2} (1 - 2\mu_v \eta_N(r)) \Delta_\rho \right], \quad (51)$$

$$V_{S.O.}^\Lambda(r) = \frac{-1}{2M_\Lambda^{*2}(r)r} \left[\Delta_\sigma^\Lambda + \Delta_\omega^\Lambda \right], \quad (52)$$

$$V_{S.O.}^{\Sigma^+}(r) = \frac{-1}{2M_\Sigma^{*2}(r)r} \left[\Delta_\sigma^\Sigma + (1 - 4\mu_s \eta_\Sigma(r)) \Delta_\omega^\Sigma + \frac{1}{2} (1 - \frac{4}{5} \mu_v \eta_\Sigma(r)) \Delta_\rho \right], \quad (53)$$

$$V_{S.O.}^{\Sigma^0}(r) = \frac{-1}{2M_\Sigma^{*2}(r)r} \left[\Delta_\sigma^\Sigma + (1 - 4\mu_s \eta_\Sigma(r)) \Delta_\omega^\Sigma \right], \quad (54)$$

$$V_{S.O.}^{\Sigma^-}(r) = \frac{-1}{2M_\Sigma^{*2}(r)r} \left[\Delta_\sigma^\Sigma + (1 - 4\mu_s \eta_\Sigma(r)) \Delta_\omega^\Sigma - \frac{1}{2} (1 - \frac{4}{5} \mu_v \eta_\Sigma(r)) \Delta_\rho \right], \quad (55)$$

$$V_{S.O.}^{\Xi^0}(r) = \frac{-1}{2M_\Xi^{*2}(r)r} \left[\Delta_\sigma^\Xi + (1 + 2\mu_s \eta_\Xi(r)) \Delta_\omega^\Xi + \frac{1}{2} (1 + \frac{2}{5} \mu_v \eta_\Xi(r)) \Delta_\rho \right], \quad (56)$$

$$V_{S.O.}^{\Xi^-}(r) = \frac{-1}{2M_\Xi^{*2}(r)r} \left[\Delta_\sigma^\Xi + (1 + 2\mu_s \eta_\Xi(r)) \Delta_\omega^\Xi - \frac{1}{2} (1 + \frac{2}{5} \mu_v \eta_\Xi(r)) \Delta_\rho \right]. \quad (57)$$

In the next Section, we will show the spin-orbit potentials for Λ , Σ^0 and Ξ^0 in ^{41}Ca and ^{209}Pb hypernuclei, which are evaluated self-consistently in the QMC model. These will be shown for the $1p_{3/2}$ hyperon configuration, for which the change in the self-consistently calculated meson mean fields is expected to be the largest among the states which have non-zero spin-orbit interactions.

4 Numerical results within the QMC model alone

In this section, we will discuss some of the results calculated in the QMC model alone, in order to extract the modifications necessary to achieve a more realistic calculation.

First, we need to specify the parameters used in the calculation. The parameters at the hadronic level, which are already fixed by the study of infinite nuclear matter and finite nuclei [2], are shown in Table 3. Concerning the parameters for the σ meson, we note that the

Table 3: Parameters at the hadronic level (for finite nuclei) [2].

field	mass (MeV)	$g^2/4\pi (e^2/4\pi)$
σ	418	3.12
ω	783	5.31
ρ	770	6.93
A	0	1/137.036

properties of nuclear matter only fix the ratio, (g_σ/m_σ) , with a chosen value, $m_\sigma = 550$ MeV. Keeping this ratio to be a constant, the value $m_\sigma = 418$ MeV for finite nuclei (hypernuclei) is

obtained by fitting the r.m.s. charge radius of ^{40}Ca to the experimental value, $r_{\text{ch}}(^{40}\text{Ca}) = 3.48$ fm [2].

Next, we show the calculated single-particle energies for $^{209}_Y\text{Pb}$ hypernuclei in Table 4. In

Table 4: Single-particle energies (in MeV) for $^{209}_Y\text{Pb}$ hypernuclei for $Y = \Lambda, \Sigma$ and Ξ . $^{209}_{\Lambda}\text{Pb}^*$ denotes the results calculated with using the scaled coupling constant, $0.93 \times g_{\sigma}^{\Lambda}(\sigma = 0)$, which reproduces the empirical single-particle energy for the $1s_{1/2}$ in $^{41}_{\Lambda}\text{Ca}$, -20.0 MeV [34]. The experimental data for $^{208}_{\Lambda}\text{Pb}$ are taken from Ref. [36]. Spin-orbit splittings are not well determined by the experiments.

	$^{208}_{\Lambda}\text{Pb}$ (Expt.)	$^{209}_{\Lambda}\text{Pb}^*$	$^{209}_{\Lambda}\text{Pb}$	$^{209}_{\Sigma^-}\text{Pb}$	$^{209}_{\Sigma^0}\text{Pb}$	$^{209}_{\Sigma^+}\text{Pb}$	$^{209}_{\Xi^-}\text{Pb}$	$^{209}_{\Xi^0}\text{Pb}$
$1s_{1/2}$	-27.0	-27.4	-35.9	-46.4	-35.8	-25.8	-33.5	-23.6
$1p_{3/2}$		-23.8	-31.9	-41.7	-32.0	-22.6	-29.7	-20.5
$1p_{1/2}$	-22.0 (1p)	-23.8	-31.9	-41.6	-31.9	-22.5	-29.7	-20.5
$1d_{5/2}$		-19.5	-27.1	-36.8	-27.6	-18.6	-25.6	-16.8
$2s_{1/2}$		-17.9	-25.4	-36.2	-25.9	-15.9	-25.1	-15.7
$1d_{3/2}$	-17.0 (1d)	-19.5	-27.1	-36.6	-27.4	-18.3	-25.6	-16.8
$1f_{7/2}$		-14.7	-21.8	-31.5	-22.6	-13.9	-21.2	-12.7
$2p_{3/2}$		-12.6	-19.4	-29.7	-20.3	-10.9	-20.4	-11.3
$1f_{5/2}$	-12.0 (1f)	-14.6	-21.7	-31.1	-22.3	-13.5	-21.3	-12.8
$2p_{1/2}$		-12.6	-19.4	-29.5	-20.1	-10.7	-20.4	-11.4
$1g_{9/2}$		-9.5	-16.0	-25.8	-17.2	-8.6	-16.7	-8.3
$1g_{7/2}$	-7.0 (1g)	-9.4	-15.9	-25.3	-16.6	-8.1	-16.8	-8.4
$1h_{11/2}$		-4.0	-9.8	-19.9	-11.5	-3.0	-12.1	-3.7
$2d_{5/2}$		-7.1	-13.2	-23.6	-14.4	-5.2	-15.8	-6.7
$2d_{3/2}$		-7.1	-13.2	-23.4	-14.1	-4.9	-15.9	-6.7
$1h_{9/2}$		-3.9	-9.7	-19.2	-10.7	-2.2	-12.2	-3.8
$3s_{1/2}$		-6.2	-12.1	-23.5	-13.2	-3.1	-15.7	-5.9
$2f_{7/2}$		-1.8	-6.9	-17.7	-8.4	—	-11.6	-2.0
$3p_{3/2}$		-1.1	-5.6	-16.9	-7.0	—	-7.4	-1.4
$2f_{5/2}$		-1.7	-6.8	-17.3	-8.0	—	-11.7	-2.0
$3p_{1/2}$		-1.1	-5.6	-16.8	-6.8	—	-7.4	-1.4
$1i_{13/2}$		—	-3.4	-13.9	-5.4	—	-7.6	—

principle, the existence of the hyperon outside of the nuclear core breaks spherical symmetry, and one should include this in a truly rigorous treatment. We neglected this effect, since it is expected to be of little importance for spectroscopic calculations [66, 67]. However, we included the response of the nuclear core arising from the self-consistent calculation, which is significant for a description of the baryon currents and magnetic moments, and a purely relativistic effect [67, 68]. Thus, we should always specify the state of the hyperon in which the calculation was performed.

Concerning the single-particle energy levels for Λ hypernuclei, although a direct comparison with the data is not precise due to the different configurations from those observed in the experiments, the calculated results seem to significantly overestimate the binding. In order to make an estimate of the difference due to this different configuration, we calculated the following quantity. By removing one $1p_{3/2}$ neutron in ^{16}O , and putting a Λ as experimentally

observed, we calculate in the same way as for $^{17}_{\Lambda}\text{O}$ - which means the nuclear core is still treated as spherical, although the core nucleus is deformed, and a rearrangement of the shell structure is expected to happen. In this case the calculated energy for the $1s_{1/2}$ Λ is -19.9 MeV, to be compared with the value -20.5 MeV of the present treatment.

At first look, the spin-orbit splittings for the Λ single-particle energies for $^{209}_{\Lambda}\text{Pb}$ almost vanish, as explained in Section 3. This is a very successful consequence of the explicit quark structure of the Λ considered in the SU(6) quark model.

We repeated the calculation using the scaled coupling constant, $0.93 \times g_{\sigma}^{\Lambda}(\sigma = 0)$, which reproduces the empirical single-particle energy for the $1s_{1/2}$ in $^{41}_{\Lambda}\text{Ca}$, -20.0 MeV [34]. The results obtained using this scaled coupling constant are denoted by $^{209}_{\Lambda}\text{Pb}^*$ in Table 4. Then, one can easily understand that the QMC model does not require a large SU(3) breaking effect (only 7 %) to reproduce the empirical single-particle energies. We should mention that a similar calculation was carried out by varying the coupling constant, g_{ω}^{Λ} . In this case, the coupling constant obtained was, $1.10 \times g_{\omega}^{\Lambda}$, to reproduce the empirical single-particle energy for the $1s_{1/2}$ in $^{41}_{\Lambda}\text{Ca}$, -20.0 MeV [34]. The calculated results with this scaled coupling constant, $1.10 \times g_{\omega}^{\Lambda}$, are almost identical to those calculated with the coupling constant, $0.93 \times g_{\sigma}^{\Lambda}$. This shows again that the QMC model does not require large SU(3) symmetry breaking to reproduce the empirical data.

Although the present treatment is based on the underlying quark structure of the nucleon and hyperon, the overestimates discussed above may be ascribed to the lack of an explicit inclusion of the Pauli principle at the quark level among the u and d quarks in the core nucleons and the Λ . If one wants to reproduce the experimental single-particle energies, one needs to include the Pauli principle at the quark level which gives some repulsion.

For Σ and Ξ hypernuclei, the situation is even more complicated. We need to take into account the effect of channel coupling, $\Sigma N - \Lambda N$ and $\Xi N - \Lambda \Lambda$, as well as Pauli blocking effect at the quark level. This is necessary to get more realistic results [15, 25, 26, 40, 43, 44, 46, 47, 48, 52, 65]. The results shown in Table 4 (and also Table 5) are obtained without including either these channel coupling effects, or the Pauli blocking effect at the quark level. These effects will be considered in specific ways at the hadronic level in Section 5.

In Table 5, we list the calculated binding energy per baryon (including hyperon), $-E/A$, r.m.s. charge radius, r_{ch} , and r.m.s. radii of the the hyperon Y and the neutron and proton distributions (r_Y , r_n and r_p , respectively), for the $1s_{1/2}$ and $1p_{3/2}$ hyperon configurations. The r.m.s. charge radius is calculated by convolution with a proton form factor [2]. For comparison, we also give these quantities without a hyperon - i.e., for normal finite nuclei. The differences in values for finite nuclei and hypernuclei listed in Table 5 reflect the effects of the hyperon, through the self-consistency procedure. One can easily see that the effects of the hyperon become weaker as the atomic number becomes larger, and as the hyperon binding energies become smaller.

Next we show in Figs. 3 and 4 the spin-orbit potentials for the hyperons, Λ , Σ^0 and Ξ^0 , in $^{41}_Y\text{Ca}$ and $^{209}_Y\text{Pb}$ hypernuclei for the $1p_{3/2}$ hyperon configuration. For comparison, we also show the spin-orbit potential for the neutron calculated self-consistently by Eq. (51), with the same configuration as the hyperon.

It is interesting to focus on some particular single-particle energy levels, e.g., $1g_{9/2}$ and $1g_{7/2}$ in $^{209}_{\Lambda}\text{Pb}$, $^{209}_{\Sigma^0}\text{Pb}$ and $^{209}_{\Xi^0}\text{Pb}$. Comparing these single-particle energies with the plotted spin-orbit potentials in Fig. 4, one can understand the origin of the reverse in magnitudes for the single-particle energies between the $^{209}_{\Sigma^0}\text{Pb}$ ($^{209}_{\Lambda}\text{Pb}$) and $^{209}_{\Xi^0}\text{Pb}$, and why the spin-orbit splittings for $^{209}_{\Sigma^0}\text{Pb}$ are the most pronounced ones among them. Although the spin-orbit potentials shown in Fig. 4 are for the $1p_{3/2}$ hyperon configuration, the main features also hold for these energy

Table 5: Binding energy per baryon, $-E/A$ (in MeV), r.m.s. charge radius, r_{ch} , and r.m.s. radii of the hyperon, r_Y , neutron, r_n , and proton, r_p (in fm) for $^{41}_Y\text{Ca}$ and $^{209}_Y\text{Pb}$. $^{41}_\Lambda\text{Ca}^*$ and $^{209}_\Lambda\text{Pb}^*$ are the results calculated with using the scaled coupling constant, $0.93 \times g_\sigma^\Lambda(\sigma = 0)$, which reproduces the empirical single-particle energy for the $1s_{1/2}$ in $^{41}_\Lambda\text{Ca}$, -20.0 MeV [34]. Double asterisks, **, indicates the value used for fitting.

hypernuclei	hyperon state	$-E/A$	r_{ch}	r_Y	r_n	r_p
$^{41}_\Lambda\text{Ca}^*$	$1s_{1/2}$	7.66	3.51	2.76	3.31	3.42
$^{41}_\Lambda\text{Ca}$	$1s_{1/2}$	7.83	3.52	2.55	3.30	3.42
$^{41}_\Sigma^+\text{Ca}$	$1s_{1/2}$	7.65	3.52	2.69	3.31	3.42
$^{41}_\Sigma^0\text{Ca}$	$1s_{1/2}$	7.83	3.52	2.52	3.30	3.42
$^{41}_\Sigma^-\text{Ca}$	$1s_{1/2}$	7.97	3.52	2.31	3.30	3.42
$^{41}_\Xi^0\text{Ca}$	$1s_{1/2}$	7.43	3.50	2.80	3.32	3.40
$^{41}_\Xi^-\text{Ca}$	$1s_{1/2}$	7.54	3.50	2.62	3.32	3.40
$^{41}_\Lambda\text{Ca}^*$	$1p_{3/2}$	7.48	3.50	3.43	3.32	3.41
$^{41}_\Lambda\text{Ca}$	$1p_{3/2}$	7.57	3.51	3.17	3.32	3.41
$^{41}_\Sigma^+\text{Ca}$	$1p_{3/2}$	7.47	3.51	3.24	3.32	3.41
$^{41}_\Sigma^0\text{Ca}$	$1p_{3/2}$	7.59	3.51	3.13	3.32	3.41
$^{41}_\Sigma^-\text{Ca}$	$1p_{3/2}$	7.70	3.51	3.02	3.31	3.41
$^{41}_\Xi^0\text{Ca}$	$1p_{3/2}$	7.30	3.49	3.58	3.33	3.39
$^{41}_\Xi^-\text{Ca}$	$1p_{3/2}$	7.40	3.49	3.36	3.32	3.39
^{40}Ca	—	7.36	3.48**	—	3.33	3.38
$^{209}_\Lambda\text{Pb}^*$	$1s_{1/2}$	7.36	5.49	3.97	5.67	5.43
$^{209}_\Lambda\text{Pb}$	$1s_{1/2}$	7.39	5.50	3.79	5.67	5.43
$^{209}_\Sigma^+\text{Pb}$	$1s_{1/2}$	7.37	5.49	4.06	5.67	5.43
$^{209}_\Sigma^0\text{Pb}$	$1s_{1/2}$	7.39	5.50	3.77	5.67	5.43
$^{209}_\Sigma^-\text{Pb}$	$1s_{1/2}$	7.41	5.50	3.42	5.67	5.43
$^{209}_\Xi^0\text{Pb}$	$1s_{1/2}$	7.32	5.49	3.82	5.68	5.43
$^{209}_\Xi^-\text{Pb}$	$1s_{1/2}$	7.34	5.49	3.48	5.68	5.43
$^{209}_\Lambda\text{Pb}^*$	$1p_{3/2}$	7.34	5.49	4.70	5.68	5.43
$^{209}_\Lambda\text{Pb}$	$1p_{3/2}$	7.37	5.49	4.50	5.67	5.43
$^{209}_\Sigma^+\text{Pb}$	$1p_{3/2}$	7.34	5.49	4.65	5.68	5.43
$^{209}_\Sigma^0\text{Pb}$	$1p_{3/2}$	7.37	5.49	4.46	5.67	5.43
$^{209}_\Sigma^-\text{Pb}$	$1p_{3/2}$	7.39	5.49	4.28	5.67	5.43
$^{209}_\Xi^0\text{Pb}$	$1p_{3/2}$	7.30	5.49	4.57	5.68	5.43
$^{209}_\Xi^-\text{Pb}$	$1p_{3/2}$	7.32	5.49	4.35	5.68	5.43
^{208}Pb	—	7.25	5.49	—	5.68	5.43

levels.

As for the spin-orbit potentials for the Σ in hypernuclei, the QMC results show a slight inequality $|V_{S.O.}^\Sigma| < |V_{S.O.}^N|$, which is indicated in Fig. 3. This contrasts with the result of Pirner [13], $|V_{S.O.}^\Sigma| = \frac{4}{3}|V_{S.O.}^N|$, but is rather similar to the results of Brockmann [23] and Dover, Millener and Gal [26].

5 Effects of Pauli blocking and channel coupling

As discussed in Section 4, we need to include the effects of Pauli blocking at the quark level, and also channel coupling, if we wish to make more realistic predictions. These effects will be considered in specific ways at the hadronic level in this Section. A more consistent treatment at the quark level is beyond the scope of the present study.

5.1 The Pauli blocking effect

Here we consider the effect of the Pauli blocking at the quark level in a specific way at the hadronic level. It seems natural to assume that this effect works repulsively in a way that the strength is proportional to the u and/or d quark baryonic (number) density of the core nucleons. Then one can expect that the u and/or d quarks in the hyperon feel a stronger repulsion at the position where the baryon density is large. As a consequence, the wave function of the hyperon (quark) will be suppressed in this region. We assume here that the Pauli blocking effect is simply proportional to the baryonic density, although one could consider a more complicated density dependence. Then, the Dirac equation for the hyperon Y , Eq. (5), may be modified by

$$[i\gamma \cdot \partial - M_Y^*(\sigma) - (\lambda_Y \rho_B(\vec{r}) + g_\omega^Y \omega(\vec{r}) + g_\rho I_3^Y b(\vec{r}) + eQ_Y A(\vec{r})) \gamma_0] \psi_Y(\vec{r}) = 0, \quad (58)$$

where, $\rho_B(\vec{r})$ is the baryonic density at the position \vec{r} in the hypernucleus due to the core nucleons, and λ_Y is a constant to be determined empirically. In the present treatment, we fitted this constant $\lambda_Y, Y = \Lambda$, to the empirical single particle energy for the $1s_{1/2}$ in $^{209}_{\Lambda}\text{Pb}$, -27.0 MeV [36]. One can regard that this fitted value also includes the attractive $\Lambda N \rightarrow \Sigma N$ channel coupling effect for the Λ single-particle energies, because the value fitted is the experimentally observed one. However, for the Σ hypernuclei, the repulsive $\Sigma N \rightarrow \Lambda N$ channel coupling effect must be included in addition to this effective Pauli blocking, in a way to reproduce the relative repulsive energy shift in the single-particle energies for the Σ . This issue will be discussed in the next Section. The fitted value for the constant λ_Λ is $\lambda_\Lambda = 60.25$ MeV (fm)³. Then for the Σ and Ξ hypernuclei, we can deduce the constants, $\lambda_{\Sigma, \Xi}$, corresponding to the effective Pauli blocking effect as, $\lambda_\Sigma = \lambda_\Lambda$, and $\lambda_\Xi = \frac{1}{2}\lambda_\Lambda$, by counting the total number of u and d quarks in those hyperons.

5.2 The effect of channel coupling

We consider here the channel coupling (strong conversion) effect additional to the Pauli blocking at the quark level. It is expected that the channel couplings, $\Sigma N - \Lambda N$ and $\Xi N - \Lambda \Lambda$, generally exist in hypernuclei, and the former coupling is considered to be especially important [15, 25, 26, 43, 44, 46, 47, 48, 52, 65].

First, we consider the $\Sigma N - \Lambda N$ channel coupling. We estimate this effect using the Nijmegen potential [71] as follows. Including the effective Pauli blocking potential, $\lambda_\Sigma \rho_B(r)$ ($\lambda_\Sigma = \lambda_\Lambda = 60.25$ MeV (fm)³), we obtain as the single-particle energy for the $1s_{1/2}$ level in

$\Sigma^0_{209}\text{Pb}$, -26.9 MeV. This value does not contain the effect of the channel coupling to the Λ . On the other hand, in a conventional first-order Brueckner calculation based on the standard choice of the single-particle potentials (cf. ref. [72] for details) the binding energy for the Σ in nuclear matter with the Nijmegen potential [71] is, 12.6 MeV, for the case without including the correct channel coupling effect to the Λ , namely, without the Pauli-projector in the ΛN channel. When the channel coupling to the ΛN is recovered and the Pauli-projector in the ΛN channel is included, the binding energy for the Σ in nuclear matter decreases to 5.3 MeV. Then, the decrease in the calculated binding energy for the Σ , $12.6 - 5.3 = + 7.3$ MeV, should be considered as a net effect of the $\Sigma N - \Lambda N$ channel coupling for the Σ . In the present study, we include the effect by assuming the same form as that was applied for the effective Pauli blocking via $\lambda_\Sigma \rho_B(r)$, and adjust the parameter $\lambda_\Sigma = \lambda_\Lambda$ to $\tilde{\lambda}_\Sigma \neq \lambda_\Sigma$ to reproduce this difference in the single-particle energy for the $1s_{1/2}$ in $\Sigma^0_{209}\text{Pb}$, namely, $-19.6 = -26.9 + 7.3$ MeV. Here we should point out that our previous study [2] shows that the baryon density around the center of the ^{208}Pb nucleus is consistently close to that of nuclear matter within the model. The value obtained for $\tilde{\lambda}_\Sigma$ in this way is, $\tilde{\lambda}_\Sigma = 110.6$ MeV (fm)³.

As for the $\Xi N - \Lambda\Lambda$ channel coupling, a study of Carr, Afnan and Gibson [48] shows that the effect is very small for the calculated binding energy for $^6_{\Lambda\Lambda}\text{He}$. The difference in the binding energy is typically less than 1 MeV for the results calculated with and without inclusion of the channel coupling effect. Although their estimate is not for large atomic number hypernuclei, nor nuclear matter, we expect that the $\Xi N - \Lambda\Lambda$ channel coupling effect is not so large for the calculation of the single-particle energies, and thus, we neglect it in the present study.

5.3 Results

Including all the effects, the Pauli blocking and the $\Sigma N - \Lambda N$ channel coupling discussed in Sections 5.1 and 5.2, we will present the final results in this Section.

In Tables 6 and 7, we list the calculated single-particle energies for $^{17}_Y\text{O}$, $^{41}_Y\text{Ca}$, $^{49}_Y\text{Ca}$, $^{91}_Y\text{Zr}$ and $^{209}_Y\text{Pb}$ hypernuclei, together with the experimental data for the Λ hypernuclei. Unfortunately, data for the larger atomic number hypernuclei are limited to Λ hypernuclei. Concerning the single-particle energy levels for the Λ hypernuclei, the QMC model supplemented by the effective Pauli blocking effect employed at the hadronic level, reproduces the data reasonably well. The small spin-orbit splittings are still achieved, as before, with the QMC model alone.

It is interesting to compare the single-particle energies for the charged hyperons, Σ^\pm and Ξ^\pm , and those of the neutral hyperons, Σ^0 and Ξ^0 . The present results imply that the Coulomb force is important for forming (or unforming) a bound state of the hyperon in hypernuclei. This was also discussed by Yamazaki et al. [65], in the context of the light Σ^- hypernuclei.

In Table 8, we show the calculated binding energy per baryon, r.m.s charge radius, r_{ch} and r.m.s. radii of the hyperon, neutron and proton distributions, r_Y , r_n and r_p , respectively. The results listed in Table 8 are calculated with the $1s_{1/2}$ hyperon configuration for all cases. Here, one can again notice the important role of the Coulomb force. For example, the binding energy per baryon, $-E/A$, for the Σ^- (Σ^+) hypernuclei is typically the largest (smallest) among the same atomic number hypernuclei, while the r.m.s. radii for the hyperon, r_Y , r_{Σ^-} (r_{Σ^+}) is mostly the smallest (largest) among the hypernuclei of the same atomic number.

Finally, we show the strengths of the scalar and vector potentials for the hyperons in $^{17}_Y\text{O}$, $^{41}_Y\text{Ca}$ and $^{209}_Y\text{Pb}$ with $Y = \Lambda$, Σ^0 and Ξ^0 in Figs. 5, and the effective masses of the nucleon and hyperon together with the baryon densities in $^{209}_\Lambda\text{Pb}$, $^{209}_\Sigma\text{Pb}$ and $^{209}_\Xi\text{Pb}$ in Figs. 6. From the baryon densities given for each hypernucleus, one can estimate the magnitude of the effective Pauli blocking and the $\Sigma N - \Lambda N$ channel coupling effect employed in the present study. Note

Table 6: Single-particle energies (in MeV) for $^{17}_Y\text{O}$, $^{41}_Y\text{Ca}$ and $^{49}_Y\text{Ca}$ hypernuclei, calculated with the effective Pauli blocking and the $\Sigma N - \Lambda N$ channel coupling. Experimental data are taken from Ref. [34]. Spin-orbit splittings are not well determined by the experiments.

	$^{16}_\Lambda\text{O}$ (Expt.)	$^{17}_\Lambda\text{O}$	$^{17}_{\Sigma^-}\text{O}$	$^{17}_{\Sigma^0}\text{O}$	$^{17}_{\Sigma^+}\text{O}$	$^{17}_{\Xi^-}\text{O}$	$^{17}_{\Xi^0}\text{O}$
$1s_{1/2}$	-12.5	-14.1	-17.2	-9.6	-3.3	-9.9	-4.5
$1p_{3/2}$		-5.1	-8.7	-3.2	—	-3.4	—
$1p_{1/2}$	-2.5 (1p)	-5.0	-8.0	-2.6	—	-3.4	—
	$^{40}_\Lambda\text{Ca}$ (Expt.)	$^{41}_\Lambda\text{Ca}$	$^{41}_{\Sigma^-}\text{Ca}$	$^{41}_{\Sigma^0}\text{Ca}$	$^{41}_{\Sigma^+}\text{Ca}$	$^{41}_{\Xi^-}\text{Ca}$	$^{41}_{\Xi^0}\text{Ca}$
$1s_{1/2}$	-20.0	-19.5	-23.5	-13.4	-4.1	-17.0	-8.1
$1p_{3/2}$		-12.3	-17.1	-8.3	—	-11.2	-3.3
$1p_{1/2}$	-12.0 (1p)	-12.3	-16.5	-7.7	—	-11.3	-3.4
$1d_{5/2}$		-4.7	-10.6	-2.6	—	-5.5	—
$2s_{1/2}$		-3.5	-9.3	-1.2	—	-5.4	—
$1d_{3/2}$		-4.6	-9.7	-1.9	—	-5.6	—
	—	$^{49}_\Lambda\text{Ca}$	$^{49}_{\Sigma^-}\text{Ca}$	$^{49}_{\Sigma^0}\text{Ca}$	$^{49}_{\Sigma^+}\text{Ca}$	$^{49}_{\Xi^-}\text{Ca}$	$^{49}_{\Xi^0}\text{Ca}$
$1s_{1/2}$		-21.0	-19.3	-14.6	-11.5	-14.7	-12.0
$1p_{3/2}$		-13.9	-11.4	-9.4	-7.5	-8.7	-7.4
$1p_{1/2}$		-13.8	-10.9	-8.9	-7.0	-8.8	-7.4
$1d_{5/2}$		-6.5	-5.8	-3.8	-2.0	-3.8	-2.1
$2s_{1/2}$		-5.4	-6.7	-2.6	—	-4.6	-1.1
$1d_{3/2}$		-6.4	-5.2	-3.1	-1.2	-3.8	-2.2
$1f_{7/2}$		—	-1.2	—	—	—	—

Table 7: Single-particle energies (in MeV) for $^{91}_Y\text{Zr}$ and $^{208}_Y\text{Pb}$ hypernuclei, calculated with the effective Pauli blocking and the $\Sigma N - \Lambda N$ channel coupling. Experimental data are taken from Ref. [36]. Spin-orbit splittings are not well determined by the experiments. Double asterisks, **, indicates the value used for fitting.

	$^{89}_\Lambda\text{Yb}$ (Expt.)	$^{91}_\Lambda\text{Zr}$	$^{91}_{\Sigma^-}\text{Zr}$	$^{91}_{\Sigma^0}\text{Zr}$	$^{91}_{\Sigma^+}\text{Zr}$	$^{91}_{\Xi^-}\text{Zr}$	$^{91}_{\Xi^0}\text{Zr}$
$1s_{1/2}$	-22.5	-23.9	-27.3	-16.8	-8.1	-22.7	-13.3
$1p_{3/2}$		-18.4	-20.8	-12.7	-5.0	-17.4	-9.7
$1p_{1/2}$	-16.0 (1p)	-18.4	-20.5	-12.4	-4.7	-17.4	-9.7
$1d_{5/2}$		-12.3	-15.4	-8.1	-0.9	-12.3	-5.4
$2s_{1/2}$		-10.8	-15.6	-6.5	—	-12.4	-3.9
$1d_{3/2}$	-9.0 (1d)	-12.3	-14.8	-7.5	-0.3	-12.4	-5.5
$1f_{7/2}$		-5.9	-10.2	-3.1	—	-7.5	-0.7
$2p_{3/2}$		-4.2	-10.1	—	—	-7.9	—
$1f_{5/2}$	-2.0 (1f)	-5.8	-9.4	-2.3	—	-7.6	-0.8
$2p_{1/2}$		-4.1	-9.9	—	—	-7.9	—
$1g_{9/2}$		—	-5.2	—	—	-3.3	—

	$^{208}_\Lambda\text{Pb}$ (Expt.)	$^{209}_\Lambda\text{Pb}$	$^{209}_{\Sigma^-}\text{Pb}$	$^{209}_{\Sigma^0}\text{Pb}$	$^{209}_{\Sigma^+}\text{Pb}$	$^{209}_{\Xi^-}\text{Pb}$	$^{209}_{\Xi^0}\text{Pb}$
$1s_{1/2}$	-27.0	-27.0**	-29.7	-19.6**	-10.0	-29.0	-19.2
$1p_{3/2}$		-23.4	-25.9	-16.7	-7.7	-25.3	-16.3
$1p_{1/2}$	-22.0 (1p)	-23.4	-25.8	-16.5	-7.5	-25.4	-16.3
$1d_{5/2}$		-19.1	-22.1	-13.3	-4.6	-21.6	-12.9
$2s_{1/2}$		-17.6	-21.7	-12.0	-2.1	-21.2	-12.0
$1d_{3/2}$	-17.0 (1d)	-19.1	-21.8	-13.0	-4.2	-21.6	-12.9
$1f_{7/2}$		-14.4	-18.2	-9.5	-0.9	-17.6	-9.2
$2p_{3/2}$		-12.4	-17.4	-7.8	—	-17.1	-8.0
$1f_{5/2}$	-12.0 (1f)	-14.3	-17.8	-9.0	-0.4	-17.7	-9.2
$2p_{1/2}$		-12.4	-17.2	-7.6	—	-17.1	-8.0
$1g_{9/2}$		-9.3	-14.3	-5.5	—	-13.6	-5.2
$1g_{7/2}$	-7.0 (1g)	-9.2	-13.6	-4.8	—	-13.7	-5.2
$1h_{11/2}$		-3.9	-4.9	-1.2	—	-9.7	-1.0
$2d_{5/2}$		-7.0	-7.5	—	—	-13.3	-3.8
$2d_{3/2}$		-7.0	-7.5	—	—	-13.3	-3.8
$1h_{9/2}$		-3.8	-4.8	—	—	-9.8	-1.0
$3s_{1/2}$		-6.1	-7.8	—	—	-8.3	-3.1
$2f_{7/2}$		-1.7	-5.8	—	—	-6.2	—
$3p_{3/2}$		-1.0	-3.4	—	—	-6.6	—
$2f_{5/2}$		-1.7	-5.8	—	—	-6.3	—
$3p_{1/2}$		-1.0	-3.3	—	—	-6.6	—
$1i_{13/2}$		—	—	—	—	-3.7	—

Table 8: Binding energy per baryon, $-E/A$ (in MeV), r.m.s charge radius, r_{ch} , and r.m.s radii of the hyperon, r_Y , neutron, r_n , and proton, r_p (in fm) for $^{17}_Y\text{O}$, $^{41}_Y\text{Ca}$, $^{49}_Y\text{Ca}$, $^{91}_Y\text{Zr}$ and $^{209}_Y\text{Pb}$ hypernuclei. The configuration of the hyperon, Y , is $1s_{1/2}$ for all hypernuclei. For comparison, we list also the corresponding results for normal finite nuclei. Double asterisks, **, indicates the value used for fitting.

hypernuclei	$-E/A$	r_{ch}	r_Y	r_n	r_p
$^{17}_\Lambda\text{O}$	6.37	2.84	2.49	2.59	2.72
$^{17}_{\Sigma^+}\text{O}$	5.91	2.82	3.15	2.61	2.70
$^{17}_{\Sigma^0}\text{O}$	6.10	2.83	2.79	2.60	2.71
$^{17}_{\Sigma^-}\text{O}$	6.31	2.84	2.49	2.59	2.72
$^{17}_{\Xi^0}\text{O}$	5.86	2.80	2.98	2.62	2.68
$^{17}_{\Xi^-}\text{O}$	6.02	2.81	2.65	2.61	2.69
^{16}O	5.84	2.79	—	2.64	2.67
$^{41}_\Lambda\text{Ca}$	7.58	3.51	2.81	3.31	3.42
$^{41}_{\Sigma^+}\text{Ca}$	7.33	3.50	3.43	3.32	3.41
$^{41}_{\Sigma^0}\text{Ca}$	7.44	3.51	3.14	3.31	3.41
$^{41}_{\Sigma^-}\text{Ca}$	7.60	3.51	2.87	3.31	3.41
$^{41}_{\Xi^0}\text{Ca}$	7.34	3.49	3.09	3.32	3.40
$^{41}_{\Xi^-}\text{Ca}$	7.45	3.50	2.84	3.32	3.40
^{40}Ca	7.36	3.48**	—	3.33	3.38
$^{49}_\Lambda\text{Ca}$	7.58	3.54	2.84	3.63	3.45
$^{49}_{\Sigma^+}\text{Ca}$	6.32	3.57	3.47	3.71	3.48
$^{49}_{\Sigma^0}\text{Ca}$	7.40	3.54	3.14	3.64	3.45
$^{49}_{\Sigma^-}\text{Ca}$	7.48	3.55	2.60	3.63	3.45
$^{49}_{\Xi^0}\text{Ca}$	7.32	3.53	3.14	3.65	3.43
$^{49}_{\Xi^-}\text{Ca}$	7.35	3.53	2.79	3.65	3.44
^{48}Ca	7.27	3.52	—	3.66	3.42
$^{91}_\Lambda\text{Zr}$	7.95	4.29	3.25	4.29	4.21
$^{91}_{\Sigma^+}\text{Zr}$	7.82	4.28	4.01	4.30	4.20
$^{91}_{\Sigma^0}\text{Zr}$	7.87	4.29	3.56	4.30	4.21
$^{91}_{\Sigma^-}\text{Zr}$	7.92	4.29	2.89	4.29	4.21
$^{91}_{\Xi^0}\text{Zr}$	7.83	4.28	3.54	4.30	4.20
$^{91}_{\Xi^-}\text{Zr}$	7.87	4.28	2.98	4.30	4.20
^{90}Zr	7.79	4.27	—	4.31	4.19
$^{209}_\Lambda\text{Pb}$	7.35	5.49	3.99	5.67	5.43
$^{209}_{\Sigma^+}\text{Pb}$	7.28	5.49	4.64	5.68	5.43
$^{209}_{\Sigma^0}\text{Pb}$	7.31	5.49	4.26	5.67	5.43
$^{209}_{\Sigma^-}\text{Pb}$	7.34	5.49	3.80	5.67	5.43
$^{209}_{\Xi^0}\text{Pb}$	7.30	5.49	3.96	5.68	5.43
$^{209}_{\Xi^-}\text{Pb}$	7.32	5.49	3.59	5.68	5.43
^{208}Pb	7.25	5.49	—	5.68	5.43

that the baryon densities versus the distance r from the center of the hypernuclei are slightly different for each hypernucleus due to the self-consistent calculations. We should also mention that the results shown in Figs. 6 are calculated by employing different parameters (and a different version of the model) from those shown in Ref. [3].

6 Summary and discussion

In summary, we have reported results for Λ , Σ and Ξ hypernuclei which were systematically calculated with the QMC model for the first time. Especially, the spin-orbit potentials for the hyperons in the hypernuclei were evaluated self-consistently with the explicit quark structure for the bound hyperon and nucleons. The very small spin-orbit force for the Λ in hypernuclei was achieved naturally in the present treatment. This is a direct consequence of the SU(6) quark model wave function for the Λ used in the QMC model. However, the single-particle energies calculated in the QMC model alone tend to overestimate the experimental data. In order to overcome this overbinding problem, we included the effect of Pauli blocking in a phenomenological way. For the Σ hypernuclei, we took into account the channel coupling effect estimated using the Nijmegen potential. In the future, these effects, which were included phenomenologically at the hadronic level in the present study, should be treated on the same footing, namely, at the quark level. For this purpose, it seems that the quark cluster model [19, 20] may offer some possibilities to include the Pauli blocking effect at the quark level. However, an application of the model to larger atomic number hypernuclei, or nuclear matter, seems to be difficult, and has not yet been carried out.

Although, there seem to be several points which could be improved in the present treatment, we would like to emphasize that, this study is the first, systematic investigation of the properties of hypernuclei based on explicit quark degrees of freedom. One of the advantages of the present study is the relatively simple nature of the QMC model, and simultaneously, its capability to give a quantitative description of the properties of finite nuclei.

Acknowledgement

We would like to thank I.R. Afnan for helpful discussions concerning the $\Xi N - \Lambda\Lambda$ channel coupling and letting us read the earlier version of the manuscript, Ref. [48]. This work was supported by the Australian Research Council. A.W.T. and K.S. acknowledge support from the Japan Society for the Promotion of Science.

References

- [1] a) P.A.M. Guichon, K. Saito, E. Rodionov and A.W. Thomas, Nucl. Phys. **A601** (1996) 349;
b) P.A.M. Guichon, K. Saito and A.W. Thomas, Australian Journal of Physics **50** (1997) 115.
- [2] K. Saito, K. Tsushima and A.W. Thomas, Nucl. Phys. **A609** (1996) 339;
K. Tsushima, K. Saito and A.W. Thomas, nucl-th/9608062, to be published in Proc. of the Int. National Symposium on *Non-Nucleonic Degrees of Freedom Detected in Nucleus*, Sep. 2-5, 1996, Osaka, Japan;
D.H. Lu, A.W. Thomas, K. Tsushima, A.G. Williams and K. Saito, ADP-97-17/T254, nucl-th/9706043, Phys. Lett. **B** (1997) submitted.

- [3] K. Saito, K. Tsushima and A.W. Thomas, Phys. Rev. C **55** (1997) 2637;
 K. Saito, K. Tsushima and A.W. Thomas, Phys. Rev. C **56** (1997) 566;
 K. Saito, K. Tsushima and A.W. Thomas, ADP-97-12/T249, nucl-th/9704047, Phys. Lett. **B** (1997) to be published;
 K. Saito, K. Tsushima and A.W. Thomas, nucl-th/9608060, to be published in Proc. of the Int. National Symposium on *Non-Nucleonic Degrees of Freedom Detected in Nucleus*, Sep. 2-5, 1996, Osaka, Japan;
 K. Saito, nucl-th/9705019, to be published in Proc. of the *International mini workshop on nuclear medium effect via nucleon induced reactions*, March 21 - 22, 1997, Kyoto, Japan;
 A.W. Thomas, ADP-97-20/T257, nucl-th/9707005, to be published in Proc. of the *Int. Conf. on Quark Lepton Nuclear Physics*, May 20 - 23, 1997, Osaka, Japan.
- [4] P.A.M. Guichon, Phys. Lett. **B200** (1988) 235.
- [5] K. Saito and A.W. Thomas, Phys. Lett. **B327** (1994) 9;
 K. Saito and A.W. Thomas, Phys. Rev. C **51** (1995) 2757;
 K. Saito and A.W. Thomas, Phys. Rev. C **52** (1995) 2789.
- [6] P.G. Blunden and G.A. Miller, Phys. Rev. C **54** (1996) 359.
- [7] X. Jin and B.K. Jennings, Phys. Lett. **B374** (1996) 13;
 X. Jin and B.K. Jennings, Phys. Rev. C **54** (1996) 1427;
 X. Jin and B.K. Jennings, Phys. Rev. C **55** (1997) 1567;
 H. Müller and B.K. Jennings, nucl-th/9706049.
- [8] J.D. Walecka, Ann. Phys. (N.Y.) **83** (1974) 491;
 B.D. Serot and J.D. Walecka, Adv. Nucl. Phys. **16** (1986) 1.
- [9] K. Tsushima, K. Saito and A.W. Thomas, ADP-97-5/T244, nucl-th/9701047, Phys. Lett. **B** (1997) submitted.
- [10] A. Bouyssy and J. Hüfner, Phys. Lett. **64B** (1976) 276.
- [11] R. Brockmann and W. Weise, Phys. Lett. **69B** (1977) 167;
 R. Brockmann and W. Weise, Nucl. Phys. **A355** (1981) 365.
- [12] W. Brückner et al., Phys. Lett. **79B** (1978) 157.
- [13] H.J. Pirner, Phys. Lett. **85B** (1979) 190.
- [14] J.V. Noble, Phys. Lett. **89B** (1980) 325.
- [15] C.B. Dover and A. Gal, Prog. Part. Nucl. Phys. **12** (1984) 171, and references therein.
- [16] B.K. Jennings, Phys. Lett. **246B** (1990) 325.
- [17] A.R. Bodmer, Phys. Rev. **141** (1966) 1387;
 R.H. Dalitz, R.C. Herndon, Y.C. Tang, Nucl. Phys. **B47** (1972) 109.
- [18] E.V. Hungerford and L.C. Biedenharn, Phys. Lett. **142B** (1984) 232.
- [19] S. Takeuchi and K. Shimizu, Phys. Lett. **179B** (1986) 197;
 M. Oka, K. Shimizu and K. Yazaki, Nucl. Phys. **A464** (1987) 700;
 K. Shimizu, Nucl. Phys. **A547** (1992) 265c.

- [20] U. Straub et al., Nucl. Phys. **483** (1988) 686.
- [21] M. Rayet, Ann. Phys. **102** (1976) 226;
M. Rayet, Nucl. Phys. **A367** (1981) 381.
- [22] J. Boguta and S. Bohrman, Phys. Lett. **102B** (1981) 93.
- [23] R. Brockmann, Phys. Lett. **104B** (1981) 256.
- [24] A. Bouyssy, Nucl. Phys. **A381** (1982) 445.
- [25] J. Johnston and A.W. Thomas, J. Phys. **G8** (1982) L105;
J. Johnston and A.W. Thomas, Nucl. Phys. **A392** (1983) 409.
- [26] C.B. Dover and A. Gal, Ann. Phys. **146** (1983) 309, and references therein;
C.B. Dover, D.J. Millener and A. Gal, Phys. Rep. **184** (1989) 1, and references therein.
- [27] D.J. Millener, C.B. Dover and A. Gal, Phys. Rev. C **38** (1988) 2700.
- [28] J. Mareš and J. Žofka, Z. Phys. **A333** (1989) 209.
- [29] J. Hao et al., Phys. Rev. Lett. **71** (1993) 1498.
- [30] D. Halderson, Phys. Rev. C **48** (1993) 581.
- [31] Y. Sugahara and H. Toki, Prog. Theor. Phys. (1994) 803.
- [32] M. Hjorth-Jensen, A. Polls, A. Ramos, H. Müther, Nucl. Phys. **A605** (1996) 458.
- [33] B. Povh, Nucl. Phys. **A335** (1980) 233.
- [34] R.E. Chrien **A478** (1988) 705c.
- [35] P.H. Pile et al., Phys. Rev. Lett. **66** (1991) 2585.
- [36] S. Ajimura et al., Nucl. Phys. **A585** (1995) 173c.
- [37] M. May et al., Phys. Rev. Lett. **78** (1997) 4343.
- [38] M. Chiapparini, A.O. Gattone and B.K. Jennings, Nucl. Phys. **A529** (1991) 589.
- [39] M. Rufa, H. Stöcker, P.-G. Reinhard, J. Maruhn and W. Greiner, J. Phys. **G13** (1987) L143.
- [40] Y. Yamamoto and H. Bandō, Prog. Theor. Phys. Supp. **81** (1985) 9;
Y. Yamamoto and H. Bandō, Prog. Theor. Phys. **83** (1990) 254.
- [41] T. Motoba, H. Bandō, R. Wünsch, J. Žofka, Phys. Rev. C **38** (1988) 1322.
- [42] E.D. Cooper, B.K. Jennings, J. Mareš, Nucl. Phys. **A580** (1994) 419;
J. Mareš and B.K. Jennings, Phys. Rev. C **49** (1994) 2472;
J. Mareš, B.K. Jennings and E.D. Cooper, Prog. Theor. Phys. Supp. **117** (1994) 415;
J. Mareš and B.K. Jennings, Nucl. Phys. **A585** (1995) 347c;
J. Mareš, E. Friedman, A. Gal, B.K. Jennings, Nucl. Phys. **A594** (1995) 311.

- [43] O. Morimatsu and K. Yazaki, Nucle. Phys. **A435** (1985) 727;
O. Morimatsu and K. Yazaki, Nucle. Phys. **A483** (1988) 493.
- [44] R. Hausmann, P.B. Siegel, W. Weise and M. Kohno, Phys. Lett. **B199** (1987) 17;
M. Kohno, R. Hausmann, P. Siegel and W. Weise, Nucl. Phys. **A470** (1987) 609;
R. Hausmann, Nucl. Phys. **A479** (1988) 247c.
- [45] T. Harada and Y. Akaishi, Phys. Lett. **B234** (1990) 455.
- [46] E. Oset, P. Fernández de Córdoba, L.L. Salcedo and R. Brockmann, Phys. Rep. **188** (1990) 79, and references therein.
- [47] I.R. Afnan and B.F. Gibson, Phys. Rev. C **41** (1990) 2787.
- [48] S.B. Carr, I.R. Afnan and B.F. Gibson, Flinders University Preprint (1997).
- [49] Joseph Cohen and H. J. Weber, Phys. Rev. C **44** (1991) 1181.
- [50] T. Harada, Nucl. Phys. **A547** (1992) 165c.
- [51] T. Yamada and K. Ikeda, Nucl. Phys. **A547** (1992) 175c.
- [52] Yoshinori Akaishi, Nucl. Phys. **A547** (1992) 217c.
- [53] N.K. Glendenning, D. Von-Eiff, M. Haft, H. Lenske and M.K. Weigel, Phys. Rev. C **48** (1993) 889.
- [54] J. Dabrowski and J. Rożyniec, Phys. Lett. **B323** (1994) 99;
J. Dabrowski, Acta Physica Polonica **B25** (1994) 575.
- [55] Prog. Theor. Phys. Suppl. **117** (1994), edited by T. Motoba, Y. Akaishi and K. Ikeda, and references therein.
- [56] F. Ineichen, D. Von-Eiff and M.K. Weigel, J. Phys. **G22** (1996) 1421.
- [57] Zhong-yu Ma, J. Speth, S. Krewald, Bao-qiu Chen and A. Reuber, Nucl. Phys. **A608** (1996) 305.
- [58] R. Bertini et al., Phys. Lett. **90B** (1980) 375;
R. Bertini et al., Phys. Lett. **136B** (1984) 29;
R. Bertini et al., Phys. Lett. **158B** (1985) 19.
- [59] H. Piekacz et al., Phys. Lett. **110B** (1982) 428.
- [60] M. Danysz et al., Phys. Rev. Lett. **11** (1963) 29.
- [61] D.J. Prowse, Phys. Rev. Lett. **17** (1963) 783.
- [62] S. Aoki et al., Prog. Thoer. Phys. **85** (1991) 1287.
- [63] K. Imai, Nucl. Phys. **A527** (1991) 181c.
- [64] Thomas Walcher, Nucl. Phys. **A479** (1988) 63c.

- [65] T. Yamazaki et al., Phys. Rev. Lett. **54** (1985) 102. T. Yamazaki, R.S. Hayano, O. Moriguchi and K. Yazaki, Phys. Lett. **B207** (1988) 393;
 R.S. Hayano et al., Phys. Lett. **B231** (1989) 355;
 R.S. Hayano et al., Nuovo Cim. **102 A** (1989) 437;
 H. Outa, T. Yamazaki, M. Iwasaki, Prog. Theor. Phys. Suppl. **117** (1994) 177.
- [66] R.J. Furnstahl and B.D. Serot, Nucl. Phys. **A468** (1987) 539.
- [67] J. Cohen, Phys. Rev. C **48** (1993) 1346.
- [68] J. Cohen and R.J. Furnstahl, Phys. Rev. C **35** (1987) 2231.
- [69] R.L. Jaffe, Phys. Rev. Lett. **38** (1977) 195.
- [70] H. Kuwabara and T. Hatsuda, Prog. Theor. Phys. **94** (1995) 1163;
 T. Hatsuda, H. Shiomi and H. Kuwabara, Prog. Theor. Phys. **95** (1996) 1009.
- [71] P.M.M. Maessen, T.A. Rijken, and J.J. de Swart, Phys. Rev. C **40** (1989) 2226.
- [72] A. Reuber, K. Holinde, and J. Speth, Nucl. Phys. **A570** (1994) 543.

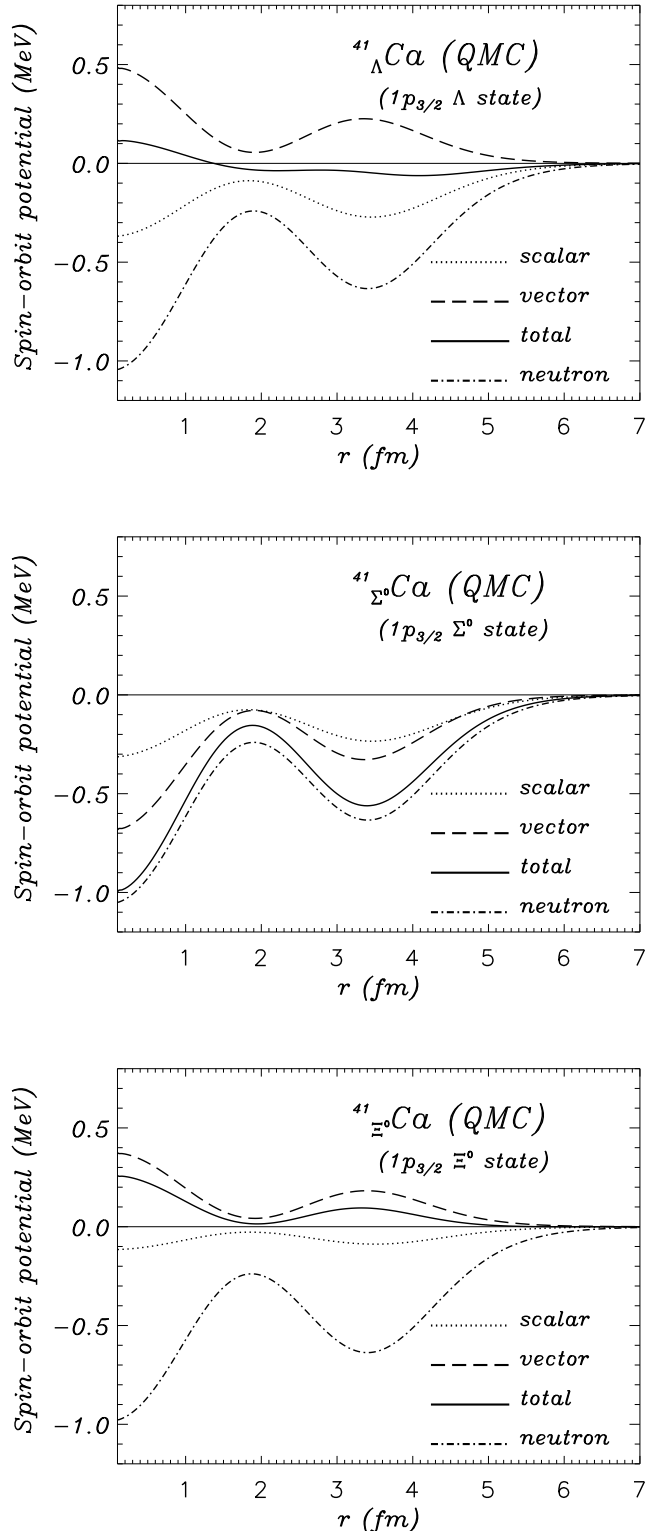


Figure 3: Spin-orbit potentials, $V_{S.O.}^Y(r)$, calculated in the QMC model alone for $Y = \Lambda$, Σ^0 and Ξ^0 in ^{41}Y Ca hypernuclei for the $1p_{3/2}$ hyperon state.

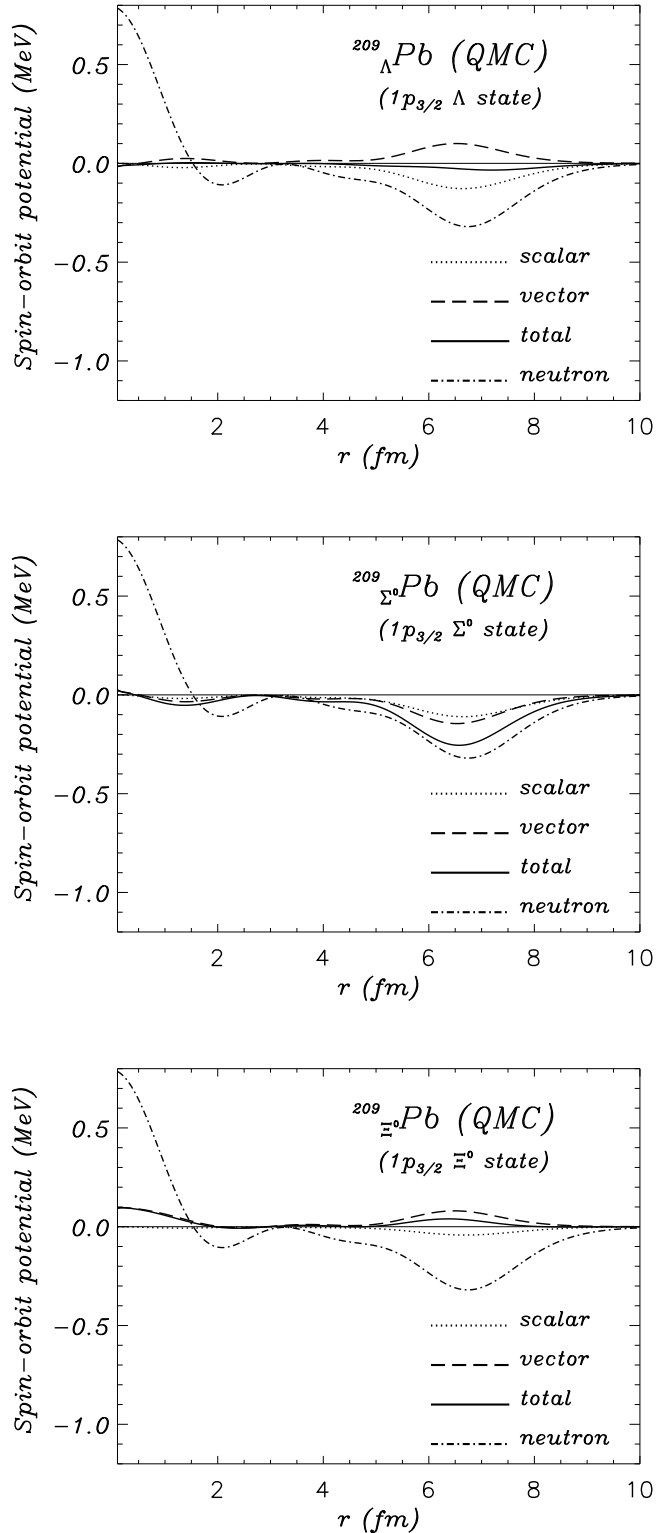


Figure 4: Spin-orbit potentials, $V_{S.O.}^Y(r)$, calculated in the QMC model alone for $Y = \Lambda$, Σ^0 and Ξ^0 in $^{209}_Y Pb$ hypernuclei for the $1p_{3/2}$ hyperon state.

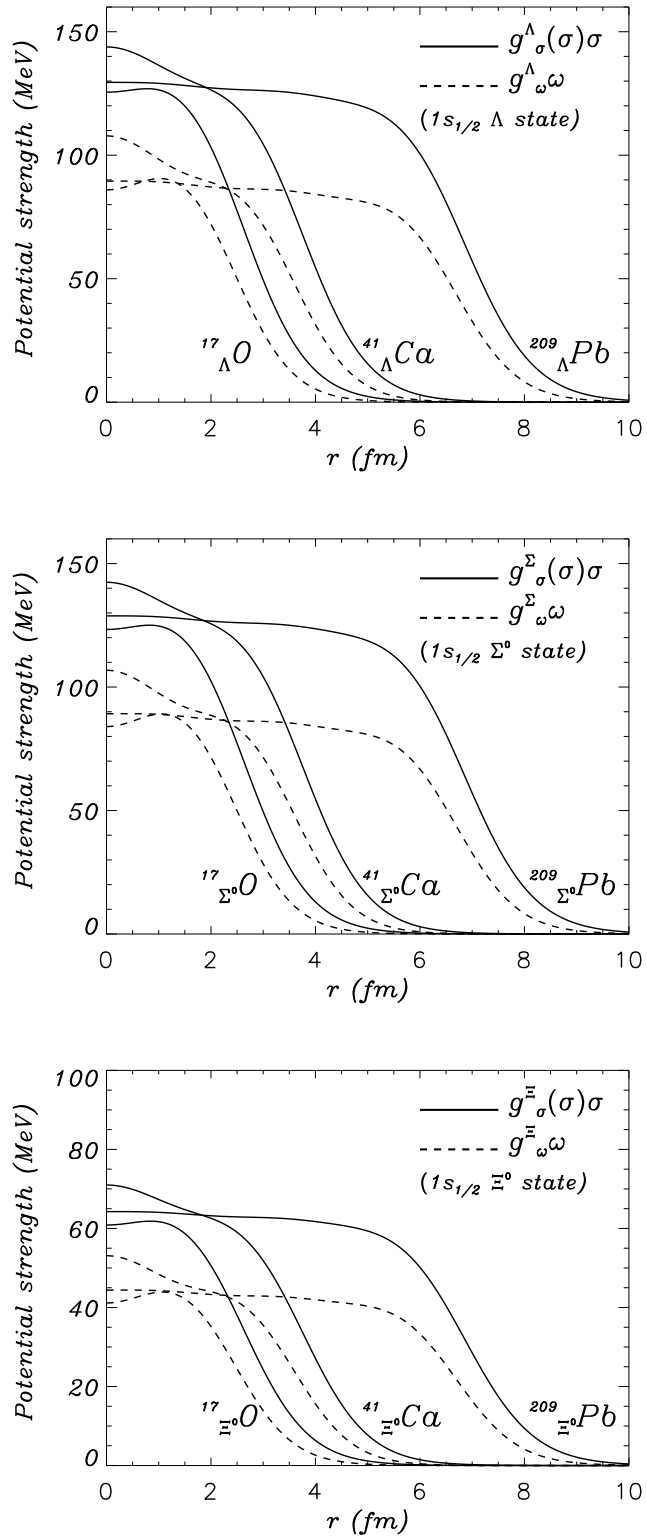


Figure 5: Potential strengths, $g_\sigma^Y(\sigma)$ and g_ω^Y , for $Y = \Lambda, \Sigma^0$ and Ξ^0 in $^{17}_Y O$, $^{41}_Y Ca$ and $^{209}_Y Pb$ hypernuclei for the $1s_{1/2}$ hyperon state, calculated with including the effects of Pauli blocking and the $\Sigma N - \Lambda N$ channel coupling.

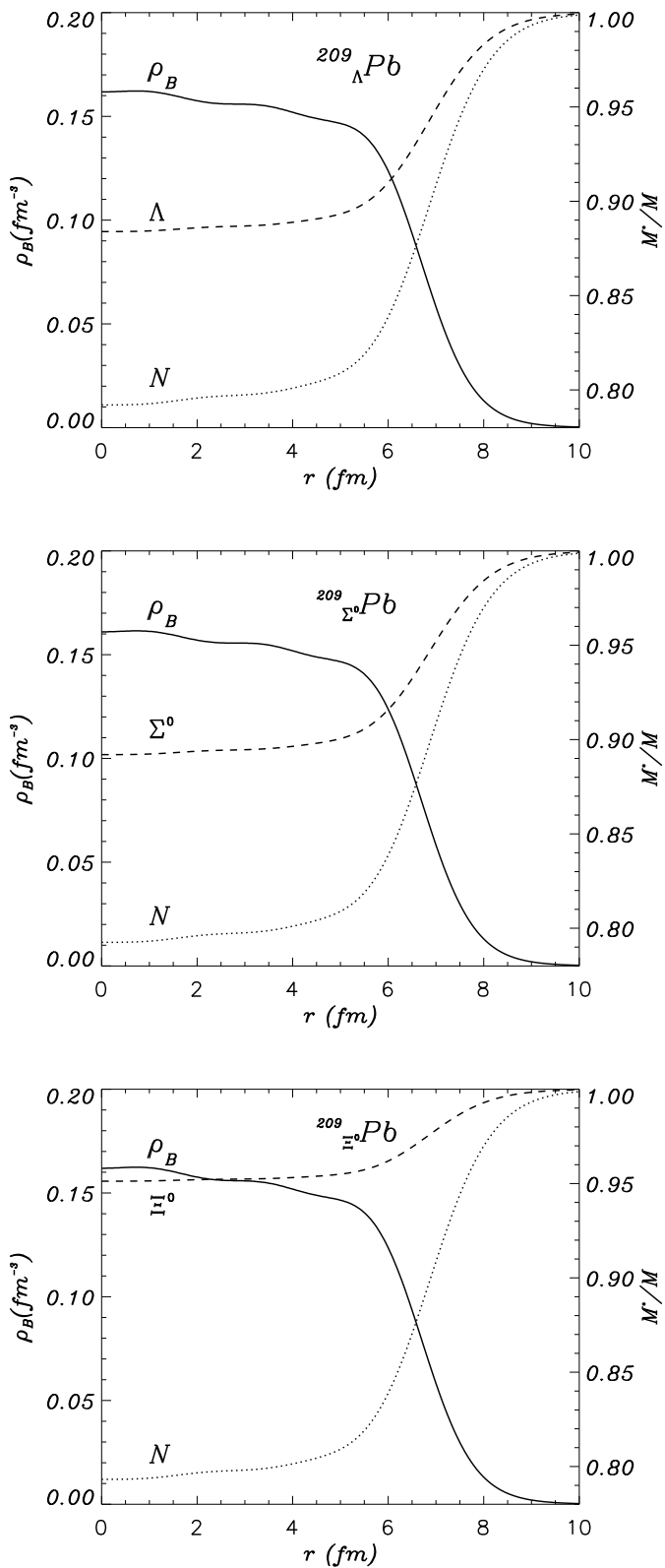


Figure 6: Effective masses of the nucleon and hyperon, and the baryon density in $^{209}_Y Pb$ hyper-nuclei for $Y = \Lambda, \Sigma^0$ and Ξ^0 . The hyperon configuration is the $1s_{1/2}$ state for all cases.